Electronic structure and the glass transition in pnictide and chalcogenide semiconductor alloys. I. The formation of the $pp\sigma$-network

Andriy Zhugayevych[1] and Vassiliy Lubchenko[1,2,a)]
[1]*Department of Chemistry, University of Houston, Houston, Texas 77204-5003, USA*
[2]*Department of Physics, University of Houston, Houston, Texas 77204-5005, USA*

(Received 3 June 2010; accepted 17 October 2010; published online 16 December 2010)

Semiconductor glasses exhibit many unique optical and electronic anomalies. We have put forth a semiphenomenological scenario [A. Zhugayevych and V. Lubchenko, J. Chem. Phys. **133**, 234504 (2010)] in which several of these anomalies arise from deep midgap electronic states residing on high-strain regions intrinsic to the activated transport above the glass transition. Here we demonstrate at the molecular level how this scenario is realized in an important class of semiconductor glasses, namely chalcogen and pnictogen containing alloys. Both the glass itself and the intrinsic electronic midgap states emerge as a result of the formation of a network composed of σ-bonded atomic p-orbitals that are only weakly hybridized. Despite a large number of weak bonds, these $pp\sigma$-networks are stable with respect to competing types of bonding, while exhibiting a high degree of structural degeneracy. The stability is rationalized with the help of a hereby proposed structural model, by which $pp\sigma$-networks are symmetry-broken and distorted versions of a high symmetry structure. The latter structure exhibits exact octahedral coordination and is fully covalently bonded. The present approach provides a microscopic route to a fully consistent description of the electronic and structural excitations in vitreous semiconductors. © *2010 American Institute of Physics*. [doi:10.1063/1.3511707]

I. INTRODUCTION

The electronic and structural excitations in amorphous semiconductors, and the interplay of these excitations, have evaded a self-consistent first-principles description for decades. Amorphous semiconductors[1–4] are important both in applications, e.g., as phase change materials,[5,6] and from the basic viewpoint. The electronic structure in a disordered lattice is fundamentally different from the venerable Bloch picture of continuous bands of allowed states separated by strictly forbidden gaps, as would be applicable in periodic solids. Although a result of multiple electron scattering, the presence of such forbidden gaps in periodic solids is also consistent with their energetic stability in that such gaps usually imply stabilized occupied orbitals. In contrast, in a disordered lattice, strict gaps in the density of states are not *a priori* allowed. Yet the electronic orbitals can still be subdivided in two relatively distinct classes[7–10] (a) extended states, in which electrons move as well-defined wave-packets and (b) localized states, whose density decays nearly exponentially away from mobility bands. Despite the many successes in applying these ideas semiphenomenologically, developing a first-principles description, in which a realistically stable aperiodic lattice and mobility gaps emerge self-consistently,[11,12] has been difficult.[13] Further compounding this difficulty, several electronic and optical peculiarities of disordered semiconductors indicate that there are effects of disorder beyond those generically expected of a mechanically *stable* disordered lattice.

We have argued[14] that, instead, it is not the aperiodicity alone, but the intrinsic *metastability* of semiconductor glasses that leads to many unique properties of these disordered solids. A glass is made by thermally quenching a supercooled liquid at a rate exceeding the typical liquid relaxation rate. A supercooled liquid can be thought of as an aperiodic crystal characterized by myriad low free energy configurations that are nearly degenerate. Molecular motions in the liquid occur via local activated transitions between these low free energy configurations,[15–17] which are accompanied by the creation of high-strain interfacial regions separating the configurations. The interfaces are *intrinsic* to the activated dynamics; their concentration, for a given quenched glass, depends (logarithmically slow) only on the time scale of the glass transition, i.e., the quench speed. According to the random first order transition theory of the glass transition,[15–18] this concentration just above the glass transition temperature on 1 h scale, T_g, is generically about $\xi^{-3} \simeq 10^{20}$ cm^{-3}, within an order of magnitude or so, depending on the specific substance. The parameter ξ denotes the cooperativity length for activated reconfigurations.

Our results indicate[14] that the high-strain regions that form when the amorphous material is made may host deep midgap electronic states of topological origin, which are centered on over- and under-coordinated atoms. These states share several characteristics with the midgap electronic states in trans-polyacetylene, which are centered on defects in the perfect alternation pattern of the double and single bonds along the polymer chains.[19] Using a semiphenomenological, coarse-grained Hamiltonian, we have established the spatial and charge characteristics of the interface-based midgap

a)Author to whom correspondence should be addressed. Electronic mail: vas@uh.edu.

states in nonpolymeric glasses. We further concluded, based on the internal consistency of the description, that the states should be present only in a limited class of glasses that satisfy the following requirements: The bonding should exhibit inhomogeneous saturation so that the transfer integrals, t, in the electronic effective tight-binding (TB) Hamiltonian $\mathcal{H} = \sum_i \epsilon_i c_i^\dagger c_i + \sum_{\langle ij \rangle} t_{ij} c_i^\dagger c_j$ should uniformly exhibit spatial variation. Nevertheless, the magnitude of the variation should be modest:[14]

$$|t'/t| \gtrsim 0.5, \tag{1}$$

where t and t' denote the upper and lower limits of the variation range. More detailed estimates[20] indicate that the lower limit on the t'/t ratio is probably smaller, i.e., 0.3 or so. Finally, the spatial variation $\delta\epsilon$ in electronegativity should not be too large:

$$|\delta\epsilon| < |t - t'|, \tag{2}$$

thus implying the material is a semiconductor, since the transfer integral t is at most a few eV. Of nonpolymeric materials, only certain chalcogen- and pnictogen-containing glasses appear to satisfy all of these requirements. On the other hand, these amorphous arsenic chalcogenides and similar materials do indeed exhibit several electronic and optical anomalies that could be accounted for by the interface-based states, in a unified fashion.[14] These anomalies include light-induced electron spin resonance (ESR) and midgap absorption,[21,22] two types of photoluminescence,[23] and field-induced ultrasonic attenuation.[24] Thus general arguments, on the one hand, and observation, on the other, seem to converge on the uniqueness of chalcogenide and pnictide glasses with regard to their potential ability to host topological midgap states. Despite this remarkable convergence, the currently available evidence for the unique interplay between electronic excitations and the metastability in those glasses must be regarded as circumstantial.

The purpose of the present effort is to test the conclusions of the semiphenomenological analysis from Ref. 14 directly, based on the local chemistry specific to amorphous chalcogenide and pnictide alloys. Our basic hypothesis for the origin of the topological midgap states in the semiconductor glasses is that these glasses represent aperiodic networks of σ-bonded p-orbitals that are only weakly hybridized, as in Fig. 1. These networks exhibit a relatively small number of intrinsic over- and under-coordinated vertices. The latter are, in fact, responsible for both the midgap states and the transition state configurations intrinsic to molecular transport in the quenched melts. In testing this hypothesis, we face the deeper question of the actual stability of aperiodic $pp\sigma$-bonded networks. Experiment shows (see below) that the enthalpy excess of a glass relative to the corresponding crystal is *less than the typical vibrational energy*, i.e., a small fraction—one percent or so—of the total bonding energy. In other words, despite their aperiodicity, glasses are nearly defect-free structures, consistent with their bulk stability, both mechanical and thermodynamic. This observation is in conflict with a common view of glasses as a reconstructed—but otherwise arbitrary—array of malcoordinated configurations and other local defects, such as vacancies. This common view would imply excess enthalpies of the order of eV per several atoms while avoiding to address the mechanism of transport in the melt.

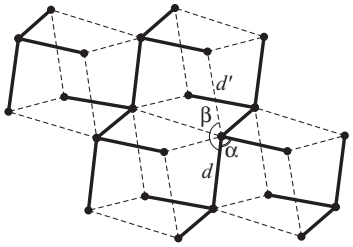

FIG. 1. Structure of rhombohedral arsenic as an example of the $pp\sigma$-bonded network. The solid lines denote regular covalent bonds that connect the central atom with the nearest neighbors, bond length d. The dashed line denote the weaker, secondary bonds connecting the central atom with its next nearest neighbors, bond length d'. Angles $\beta < 180^\circ$ and $\alpha \neq 90^\circ$ reflect the deviation from ideal octahedral coordination. These particular crystal fragment and view are based on Fig. 1 of Shang *et al.* (Ref. 25).

In the present and companion article,[20] we test the hereby proposed microscopic picture in two relatively separate stages. The present article is devoted to the first stage, in which we argue that $pp\sigma$-networks can represent the quenched liquid and frozen glass forms of these substances in the first place. We will make a case that (a) such networks are stable against other types of bonding in a rather large class of amorphous compounds containing elements from groups 15 and 16, and (b) despite their relative stability, aperiodic $pp\sigma$ networks are multiply degenerate, as are the actual liquids and glasses in question. The present work thus contains, to our knowledge, the first chemical bonding theory of a bulk glass.

The article is organized as follows. In Sec. II, we discuss in detail several key features of $pp\sigma$ networks, including their spatial nonuniformity and a hierarchy of bonding, from strictly covalent to weaker "secondary" to weaker yet van der Waals. Despite the presence of such weak bonds, the $pp\sigma$ networks are stable. To trace the origin of this stability, we formulate a structural model in Sec. III, by which both periodic and *aperiodic* $pp\sigma$-networks are symmetry-broken versions of a highly symmetric, strongly bonded structure. This view is similar, but distinct from the common view of many elemental solids as Peierls distorted simple-cubic (sc) lattices.[26] The symmetry breaking is driven by several competing interactions, including in particular sp-mixing; these, nevertheless, are only strong enough to perturb but not qualitatively modify the basic $pp\sigma$ bonding. We will verify that the resulting aperiodic $pp\sigma$-bonded lattice satisfies the three requirements for the existence of the topological states listed above. Importantly, this lattice will be argued to exhibit multiply degenerate configurations that differ by precise coordination of individual atoms, consistent with the possibility of activated transport in the corresponding quenched melts. The precise degree of degeneracy and the possibility of activated transport are both intimately related to the questions of the concentration of the corresponding transition-state configurations in the melt and the accompanying electronic excitations. The latter questions are analyzed in the companion article.[20]

II. $pp\sigma$-BONDED SEMICONDUCTORS: THE ROLE OF THE SECONDARY $pp\sigma$-INTERACTION

The goal of this Section is to provide a detailed description of $pp\sigma$-networks in pnictides and chalcogenides, as arising from sigma-bonding between p-orbitals that are only weakly sp–hybridized. Such a description is necessitated by the lack of systematic comparative studies of the electronic properties of chalcogenide and pnictide alloys, even though their structure itself has received much attention.[3,27] The $pp\sigma$-bonding emerges subject to competition from other types of local ordering. The presence of several competing types of local ordering in chalcogenides is evidenced by their broad range of structural and electronic properties, as could be seen by comparing, e.g., As_2Se_3[28] and $GeSe_2$.[29] While the former exhibits a distorted octahedral coordination and well separated s and p bands, the latter displays tetrahedral ordering and overlapping sets of s and p orbitals. At the same time, the two substances exhibit opposite trends in terms of intrinsic and light-induced ESR response.[21,22,30,31] Such simultaneous trends are particularly vivid in the Ge_xSe_{1-x} series[32] for $1/3 < x < 1/2$, which exhibit coordination ranging from tetrahedral (smaller x) to distorted octahedral (larger x). In this series, the octahedral ordering seems to correlate with the separation between s and p bands[33,34] and light-induced ESR, and anticorrelate with the presence of unpaired spins[31] and the glassforming ability.[35] Vice versa, the tetrahedral bonding exhibits the opposite trend.

When sp-hybridization is weak, each atom exhibits a distorted octahedral coordination, as exemplified in Fig. 1: Two or three nearest neighbors are situated at the distance of the regular covalent bond in an almost right-angled geometry. Opposite to each of these covalently bonded neighbors, there is an atom at a distance that exceeds the sum of the corresponding covalent radii, but is closer than the sum of the corresponding van der Waals radii.[36] *Crystalline* As, Se, As_2Se_3, GeSe are typical examples of this type of coordination. It is appropriate to think of crystals that exhibit distorted octahedral coordination not as fully covalently bonded, but as networks consisting partially of fully covalent bonds and weaker, closed-shell interactions. In the physics literature, it is customary to call the stronger bonds "front bonds" and to call the weaker bonds "back bonds."[37–39] Because the back bonds formally correspond to closed-shell interactions, chemists call them secondary bonds,[40–43] or donor–acceptor interactions,[44] or, sometimes, hypervalent or three-center bonds, where the distinction is only quantitative, if any.[42] Importantly, the secondary bonds are stronger than van der Waals interaction and are *directional*, similarly to their strictly covalent counterparts.[40] We will see that, in fact, the distinction between the secondary and covalent bonds in $pp\sigma$-networks is not sharp. A common example of the coexistence of covalent and secondary bonding is crystalline As_2Se_3, which consists of puckered layers of $AsSe_3$ pyramids, see also Figs. 7–9 below, whereby the layers are only loosely bonded. The pyramids are made of the stronger, covalent bonds, while the secondary $pp\sigma$-interaction accounts for the rest of the intralayer bonding, see Fig. 2. The interlayer secondary bonds are even weaker; nevertheless they have been argued to be as strong as 0.3 eV in As_2Se_3,[45] i.e., significantly stronger than a typical van der Waals-like bond.

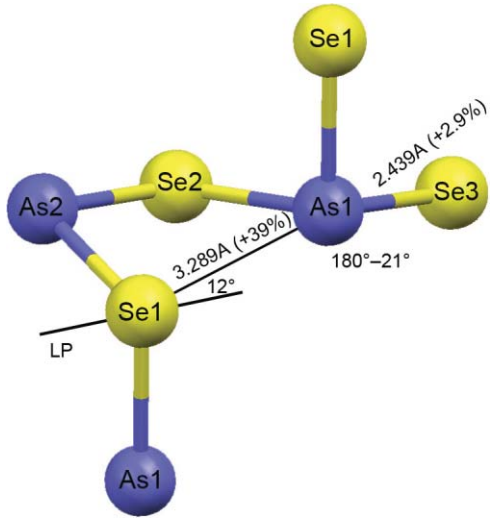

FIG. 2. A fragment of the As_2Se_3 crystal. The secondary bond between As1 and Se1 is shown with a thin solid line. The deviation from the strict octahedral coordination is reflected in different values of covalent and secondary bond strengths: $t'_\sigma/t_\sigma = 0.44 < 1$, a deviation from their strict alignment $\Delta\beta = 180^\circ - \beta = 21^\circ$, and bond elongation relative to the sum of the covalent radii: $\delta d = +0.07$ Å, $\delta d' = +0.9$ Å. The notations are the same as in Fig. 1.

Despite thousands of documented instances of secondary bonding and the similarity in its properties across a broad spectrum of compounds,[41,42,44] both the mechanism and quantitative description of this type of bonding still appear to be a subject of debate.[41] Without claiming full generality, here we will presume the existence and universality of secondary bonds based on those myriad documented cases. The energetic and spatial characteristics of these bonds will be treated empirically, using tight-binding (TB) formalism. Such an approach is controllable insofar as the substances in question are insulators or poor conductors since under these circumstances,[46] both localized, Wannier-like and the delocalized Mulliken–Hund orbitals form a complete set of electronic wave-functions. Consistent with the closed-shell character of the secondary bonding, the TB expression for the corresponding binding energy contains exclusively interaction between occupied and unoccupied orbitals of the constituent molecules. Indeed, a one-electron Hamiltonian that describes the interaction of two molecules, A and B, can be written as a block matrix, where the ket corresponding to the wave-function is a vertical stack of the kets pertaining to molecules A and B:

$$\mathcal{H} = \begin{pmatrix} \mathcal{H}^{\mathrm{A}} & V^{+} \\ V & \mathcal{H}^{\mathrm{B}} \end{pmatrix}, |\psi\rangle = \begin{pmatrix} |\psi^{\mathrm{A}}\rangle \\ |\psi^{\mathrm{B}}\rangle \end{pmatrix}. \quad (3)$$

Matrices $\mathcal{H}^{\mathrm{A}}$and $\mathcal{H}^{\mathrm{B}}$ are the Hamiltonians of the isolated molecules A and B, while V contains the corresponding transfer integrals. According to the standard perturbative expression,[47] the binding energy of two closed-shell

TABLE I. Transfer integrals (in eV) in particular crystalline forms of several elements often present in chalcogenide alloys (Ref. 39). All integrals are for the nearest neighbors, except t'_σ. In t_{ss} and t_{sp}, the subscripts indicate the constituent orbitals. Here, t_σ and t'_σ denote the transfer integrals for the covalent and secondary $pp\sigma$ bonds, and t_π for the $pp\pi$ interaction. A graphical summary of the transfer integral definitions is given in Fig. 11(a), see also p. 23 of Ref. 37.

	$-t_{ss}$	t_{sp}	t_σ	t'_σ	$-t_\pi$	Reference structure
Ge	1.70	2.36	2.56	Negligible	0.67	Diamond-Ge
As	1.17	1.60	3.10	1.66	0.79	α-As
Se	1.11	2.10	3.37	0.64	0.92	Trigonal-Se

molecules A and B, $E_{\rm bind} \equiv E^{\rm AB}_{\rm tot} - E^{\rm A}_{\rm tot} - E^{\rm B}_{\rm tot}$ reads:

$$E_{\rm bind} \approx 2\left\{\sum_n^{\rm A_{occ}}\sum_m^{\rm B_{unocc}} - \sum_n^{\rm A_{unocc}}\sum_m^{\rm B_{occ}}\right\}\frac{|V_{nm}|^2}{E^{\rm A}_n - E^{\rm B}_m}, \tag{4}$$

where $\mathcal{H}^{\rm A}|\psi^{\rm A}_n\rangle = E^{\rm A}_n|\psi^{\rm A}_n\rangle$ and $\mathcal{H}^{\rm B}|\psi^{\rm B}_n\rangle = E^{\rm B}_n|\psi^{\rm B}_n\rangle$. Labels "occ" ("unocc") denote summation over occupied (unoccupied) orbitals of the molecules A and B.

Now, the precise geometry of the $pp\sigma$-network is subject to several competing interactions, combined with the precise stoichiometry and other many body effects: the $pp\sigma$-interaction, sp-mixing, and $pp\pi$-interaction, such as often found in conjugated polymers. (See Harrison[37] for an introduction to tight-binding methods.) All these interactions have comparable strength as can be inferred from the values of the corresponding electron transfer integrals. Table I compiles the values of these transfer integrals for important representatives from groups 14, 15, and 16. Elements of these groups are of particular interest in the context of amorphous semiconductors, because of comparable electronegativity and suitable valency, of course. The close magnitude of the listed competing interactions implies that the local order, which in turn is strongly affected by the stoichiometry, plays a crucial role in determining which interaction will ultimately dominate.

One may list several complementary ways to establish the presence and significance of $pp\sigma$-bonding. A $pp\sigma$-network reveals itself structurally in a weak deviation from the octahedral coordination. In addition to a nearly right-angled geometry, the disparity between the lengths of the secondary and covalent bonds should be modest. In the latter case, the ratio of the corresponding transfer integrals, t'_σ/t_σ, is not too small, implying a relatively uniform, stable network. Furthermore, in view of a nearly universal relation $-t_\pi/t_\sigma \simeq 1/4$, Ref. 48, a large enough value of t'_σ/t_σ automatically guarantees that the effect of $pp\pi$ interactions on the geometry is small. On the other hand, when sp mixing is weak and little ss bonding is present, the top of the valence band consists primarily of p-orbitals, while the s and p subbands are relatively well separated. Indeed, consider for the sake of argument two identical centers, each having one s and p orbital and three electrons. The p-orbitals are aligned. Within the second order in the sp-mixing, the one-electron energies of the four resulting molecular orbitals are given by $\epsilon_s \mp t_{ss} - t^2_{sp}[\epsilon_p - \epsilon_s \pm (t_\sigma + t_{ss})]^{-1}$ for the $ss\sigma$ bond and $\epsilon_p \pm t_\sigma + t^2_{sp}[\epsilon_p - \epsilon_s \pm (t_\sigma + t_{ss})]^{-1}$ for the $pp\sigma$ bond. If the s and p orbitals are sufficiently separated in energy, it follows automatically that (a) the centers are $pp\sigma$-bonded and (b) the effect of the sp-mixing on the $pp\sigma$ transfer integral of the bond is small: $t_{sp}/\sqrt{t_\sigma(\epsilon_p - \epsilon_s)} < 1$. A combination of the photoemission spectra with tight-binding calculations, using the known crystal structures, strongly suggests that exactly this type of bonding occurs in the crystals of several archetypal chalcogenides: As_2S_3, As_2Se_3, and As_2Te_3.[49]

In Table II, we compile data on the deviation from the ideal octahedral coordination and the corresponding $pp\sigma$ transfer integrals, in several distinct compositions and stoichiometries characteristic of common chalcogenide and pnictide alloys. One observes that a high value of t'_σ/t_σ is indeed characteristic of $pp\sigma$-bonded materials, whereby the angular deviation from the ideal coordination does not exceed 10°. Conversely, a large value of the t'_σ/t_σ ratio, alone, is often a good predictor of $pp\sigma$-networking. Note also a subtle, but nevertheless significant trend that in such a network, the stronger bonds are somewhat *longer* than the sum of the covalent radii. Furthermore, this deviation is the more significant, the shorter—and hence stronger—are the secondary bonds. This anticorrelation is a telltale sign of "trans-influence"[42] in which the weaker bonded atom donates electrons into antibonding orbitals of the stronger bond, a common feature with secondary and donor–acceptor interactions. For the trans-influence to take place, it is essential that the counterpart covalent and secondary bonds be in a near linear geometry so that the antibonding orbital on the stronger bond overlap significantly with the bonding orbital on the secondary bond.[40] Note that tight-binding descriptions are consistent with the trans-influence. Indeed, we show in Appendix B that the bond order[65] for the AB dimer from Eq. (4) is approximately given by the expression

$$b_{\rm AB} \approx 4\left\{\sum_n^{\rm A_{occ}}\sum_m^{\rm B_{unocc}} + \sum_n^{\rm A_{unocc}}\sum_m^{\rm B_{occ}}\right\}\frac{|V_{nm}|^2}{\left(E^{\rm A}_n - E^{\rm B}_m\right)^2}. \tag{5}$$

The first (second) double sum is twice the occupation of the antibonding orbitals of molecule B (A), as donated by the bonding orbitals of A (B), consistent with the donor–acceptor nature of the secondary bond. Alternatively, according to Eq. (4), the bond order strongly correlates with the binding energy. Since the sum of the bond orders on a given atom equals to the atom's valency, stronger secondary bonds imply weaker counterpart covalent bonds.

We should point out that a large value of the t'_σ/t_σ ratio and the perfect octahedral coordination, separately or together, are often indicative but do not guarantee that the $pp\sigma$-bonding is the main contributor to the lattice stabilization. An obvious counterexample is provided by ionic compounds with the rocksalt structure, which exhibit the perfect octahedral coordination. Incidentally, using stoichiometry to impose a (distorted) rocksalt structure is not guaranteed to produce a $pp\sigma$-network either. For instance, whereas GeSe does indeed exhibit distorted octahedral coordination, AsSe forms a molecular crystal composed of As_4Se_4 units, whose symmetry is incompatible with uniform octahedral coordination, despite relatively strong secondary bonding, see Table II and the Supplemental Material.[116] Finally, other competing types of local order are present in solids formed by

TABLE II. Geometry (notations from Fig. 1) and tight-binding parameters of representative compounds in crystalline form. Lower entries correspond to progressively weaker $pp\sigma$-bonding. Here, $\bar{\alpha}$ is the average bond angle (hybridization), ϵ is the half-difference in absolute electronegativities, Δd and $\Delta d'$ are the deviations of covalent and secondary bond lengths from the sum of the covalent radii, $\Delta\beta = 180 - \beta$ is the deviation from a linear geometry, t'_σ/t_σ is the ratio of $pp\sigma$ integrals for secondary and covalent bonds. Crystallographic abbreviations: h – hexagonal, m – monoclinic, o – orthorhombic, r – rhombohedral, t – trigonal. The computational details are given in Appendix A.

Crystal and Ref.		$\bar{\alpha}$,°	ϵ,eV	Δd,Å	$\Delta d'$,Å	$\Delta\beta$,°	t'_σ/t_σ
			Strong $pp\sigma$-secondary bonding/hypervalency				
As_2Te_3	50	90.8	0.1	0.1–0.4	0.4–1.2	3–21	0.4–0.9
r-As	(51)	96.7	0	0.12	0.7	16	0.65
			Moderate $pp\sigma$-secondary bonding				
o-As	(52)	97.0	0	0.09	0.9	14	0.5
GeSe	(53)	97.0	0.7	0.18	0.9	17	0.5
t-Se at 5 GPa	(54)	104.7	0	0.05	0.8	15	0.45
As_2Se_3	(55)	97.5	0.3	0.02–0.08	0.9–1.4	10–20	0.2–0.4
As_4Se_4	(56)	98.4	0.3	−0.04+0.11	1.1–1.5	2–15	0.2–0.4
t-Se at 0 GPa	(54)	103.1	0	0.03	1.1	19	0.3
r-Se	(57)	101.1	0	0.02	1.1	9	0.3
Br at 5 K	(58)	–	0	0.02	1.0	10	0.3
Br at 250 K	(58)	–	0	0.01	1.1	10	0.3
α-m-Se	(59)	105.6	0	0.00	$\gtrsim 1.1$	–	$\lesssim 0.2$
As_2O_3 (As)	(60)	96.5	1.1	0.0–0.1	1.2	23	0.3
$AsBr_3$ (As)	(61)	99.0	1.1	−0.1+0.1	1.6	11	0.2
			sp^3-bonding				
$GeSe_2$ (Ge)	(62)	109.4	0.7	−0.06–0.03	$\gtrsim 1.3$	8	<0.3
h-Ge	(63)	109.4	0	−0.03	1.6	0	0.2
diamond-Ge	(64)	109.5	0	0	2.2	30	0.1

the elements from groups 14–16. For instance, in $GeSe_2$ the coordination of Ge atoms is tetrahedral, see Table II. Elemental phosphorus and sulfur at ambient conditions exist as molecular crystals made of tetraphosphorus P_4 and octasulphur S_8, respectively, that show no signs of octahedral coordination.

Apart from the stoichiometry and peculiar types of local ordering, the actual degree of stabilization of the $pp\sigma$-network crucially depends on the strength of the secondary bonds since they account for at least a half of the total bonds. We are not aware of systematic *ab initio* studies of the dependence of the strength of these bonds on the bond length and the deviation from the precise octahedral coordination, in a crystal. Such studies are understandably difficult, as the actual chalcogenide crystal structures exhibiting this type of bonding are very complicated. For instance, the unit cell of As_2Se_3 has 20 atoms.[45] Despite these complications, it is possible to obtain an accurate estimate of the strength of $pp\sigma$ secondary bonding in semiconductors by analyzing the simplest possible micro- and macromolecular systems that exhibit this type of bonding, i.e., dimers of diatomic halogen molecules and halogen crystals, respectively. Specifically, bromine is an appropriate example, because the elements of interest are located in periods three through five. The ground state geometry of the bromine dimer is shown in Fig. 3. Here the $pp\sigma$ molecular orbital of the lhs molecule is mixed with the in-plane $pp\pi$ molecular orbitals of the rhs molecule, as can be seen directly in the electronic density distribution in Fig. 3. Consistent with this mixing, the strength of the $pp\sigma$ secondary bond between the bromine molecules exceeds 0.3 eV, i.e., significantly more than expected of a typical van der Waals bond. According to the estimates on a variety of pseudo-dimer structures by Anderson *et al.*[67], the strength of the secondary bonding, relative to the covalent bonding, decreases toward the rhs in each period. The above figure for the binding energy of the bromine dimer, thus, gives us a secure lower bound on the strength of a secondary bond, consistent with the data in Table II. Furthermore, bromine *crystals* are comprised of layers in which Br_2 units are arranged in nearly the same geometry as in the

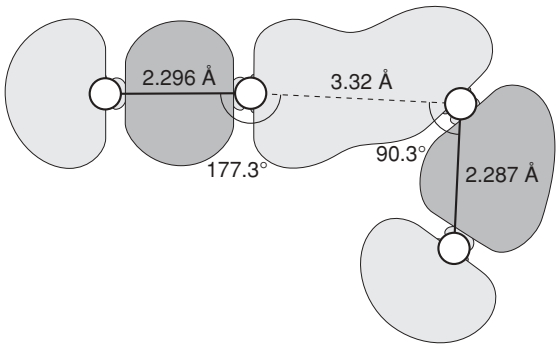

FIG. 3. A dimer of Br_2 molecules. The geometry is optimized at the MP2 level, using the program FIREFLY (Ref. 66) with aug-cc-pVTZ basis set and RHF wave-function. The gray shapes show the lowest energy molecular orbital consisting of the valence p orbitals of the Br_2 molecules (61st MO, Table V in Appendix B), see also the MO diagram in Fig. 12. The two hues reflect the sign of the wave-function. The computational details are provided in Appendix B.

ground state of an isolated pair of Br_2 molecules, see Supplementary Material.[116]

III. $pp\sigma$-NETWORKS AS SYMMETRY-BROKEN STATES

Here we propose a specific structural model of $pp\sigma$-network formation, both periodic and aperiodic, and argue that aperiodic $pp\sigma$-networks are consistent with (a) the structural degeneracy of the corresponding solid and (b) the restrictions on the magnitude of the spatial variation of the electronic transfer integral from Eq. (1) derived in Ref. 14.

In liquids and glasses, the first coordination shell is determined by the stronger bonds and is very similar to the first coordination shell in the corresponding crystals.[69–71] Much less is known about the precise configurations of the weaker-bonded, next-nearest neighbors. A useful cue is provided by the observation that the crystalline photoemission spectra of several archetypal $pp\sigma$-bonded chalcogenides—As_2S_3, As_2Se_3, and As_2Te_3[49,72] are very similar to their amorphous counterparts. In this and in Sec. IV, we argue that, indeed, the local interactions specific to $pp\sigma$-bonded glasses are of the same origin as in the corresponding crystals: In both cases, the local structures result from a symmetry-lowering transition from the perfect octahedral coordination and thus are comparably stable. The main corollary of this inference is that a supercooled liquid or quenched glass can be sufficiently stabilized by the $pp\sigma$-network alone. The key distinction between the crystal and glass is that owing to its aperiodicity, the glass is necessarily structurally degenerate.

Let us begin with crystals. It is long appreciated[36,73–75] that the structures of many polymorphs of elemental pnictogens, chalcogens, and halogens can be regarded as distorted sc, with the exception of several of the lightest elements, such as nitrogen or oxygen, which form molecular crystals. Upon increasing pressure to several tens of GPa, the structures approach the ideal octahedral coordination, while phosphorus and arsenic actually exhibit a continuous transition to the simple cubic structure (Ref. 76 and references therein). Specifically in arsenic, which is rhombohedral (A7) at ambient conditions, as the bond angles approach the right-angled geometry, the ratio of bond lengths of the nearest to the next nearest neighbor grows.[68] These two bond types correspond to the covalent and secondary bonds respectively. In the vicinity of the transition, the covalent bond *increases* in length, while the secondary bond continues to shorten,[68] see Fig. 4. Landrum and Hoffmann provide correlation data on thousands of pnictogen and chalcogen compounds that clearly demonstrate similar trans-influence between the covalent and secondary bonds,[42] see inset of Fig. 4. The molecular fragments in question are of the type X–Q–X, where Q = Sb, Te and X = F, Cl, Br, I. Note the correlation in the inset of Fig. 4 pertains to valencies 3 (2) for Sb (Te). The combined view of Fig. 4 implies that the distinction between the covalent and secondary bonds is not sharp, but is subject to precise local coordination and/or bond tension. In the strict sc limit, both the secondary and covalent bonds become equivalent and should be regarded as fully covalent, albeit hypervalent.[43] Similarly in halide

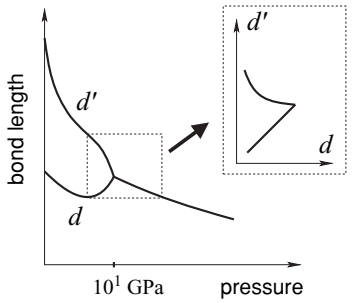

FIG. 4. Pressure dependence of the lengths of the covalent (d) and secondary (d') bond in rhombohedral arsenic, after Silas *et al.* (Ref. 68). At a critical pressure, of about 10^1 GPa, the lattice becomes simple cubic, while the two types of bonds become equivalent. In the inset, we replot the framed region with d as a function of d' and the pressure as a dummy parameter. The resulting dependence illustrates the trans-influence of the covalent and secondary bonds, cf. Figs. 1 and 2 of Landrum and Hoffmann (Ref. 42).

crystals, each $pp\sigma$-bonded layer transforms into a square lattice at a sufficiently high pressure (80 GPa for bromine[75]). Isovalent binary compounds $A^{IV}B^{VI}$ transform into the simple cubic structure not only upon increasing pressure, but also upon increasing the temperature.[77]

To rationalize these observations, we hereby propose the following *structural model*, which draws heavily on Burdett and co-workers' view of the structure of rhombohedral arsenic, black phosphorus and other compounds,[78,79] see Fig. 5. Place the atoms at the vertices of the cubic lattice, so that each atom is exactly octahedrally coordinated and the p orbitals are aligned with the principal axes. All atoms are linked, the links corresponding to bonds. Remove links so that each atom obeys the octet rule, while making sure the remaining bonds on each vertex are at 90°, not at 180°. This procedure could be interpreted as adding electrons to a rocksalt-like compound while breaking bonds, whereby each filled antibonding orbital transforms into a lone pair of electrons pointing away from the remaining bonds.[78] As a result, each pnictogen and chalcogen, for instance, will be three- and two-coordinated respectively, whereby all links pointing from an atom are at right angles. We call the resulting lattice the "parent structure." Third, estimate the energy of the resulting parent structure, using a tight-binding Hamiltonian, while assuming that the transfer integrals are significant only for the linked atoms. Now, those bond-breaking patterns that have a particular low energy are special. One should expect that to these special structures, there correspond crystals of actual substances that exhibit a distorted octahedral coordination, in which the covalent bonds will precisely correspond to the links, while the missing links correspond to secondary bonds or weaker, van der Waals interactions. For instance, Burdett and McLarnan have shown there are 36 inequivalent ways to arrange three-coordinated atoms on the cubic lattice with a repeat unit of size $2 \times 2 \times 2$. Two of the structures correspond to the lattices of black phosphorus and rhombohedral arsenic.[78] In actual materials, both of these lattices consist of double layers that are buckled and mutually shifted, compared with the parent simple cubic structure. Other specific examples can be found in Refs. 78, 79, and 80. It is understood that although the simple cubic lattice is a convenient parent

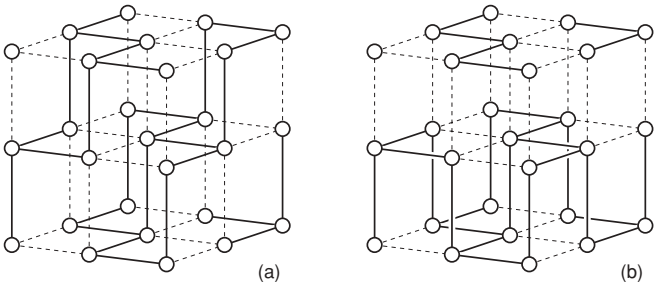

FIG. 5. Parent structures of the crystals of (a) elemental arsenic and (b) black phosphorus, after Burdett and McLarnan (Ref. 78).

structure for many compounds, it is by no means unique in this regard. For instance, Albright *et al.*[81] mention two additional *formal* ways to obtain the arsenic structure, i.e., by adding two electrons per atom to wurzite ZnS or by puckering graphite sheets. Yet what distinguishes the sc-like parent structure is that, like the actual material, it is $pp\sigma$-bonded, whereas the orbitals in the wurzite and graphite structures are sp^3 and sp^2 hybridized, respectively. We point out that IV–VI compounds that are isoelectronic with arsenic can be obtained from the parent structures of arsenic or phosphorus, see Fig. 6. Finally, note that the above rules for bond placement, i.e., three-coordinated pnictogens and two-coordinated chalcogens with right angles between bonds, can be formally regarded as a subcase of the 64-vertex model,[82] which is the 3D generalization of the venerable six-vertex model of ice and eight-vertex model of antiferroelectrics.[83] In the present case, eight configurations on pnictogen vertices and 12 configurations on chalcogen vertices have finite energies, while the rest are infinitely costly. This analogy implies that the proposed model is generalizable to more complicated coordinations by assigning finite energies to the latter.

The present structural model can be formulated for stoichiometries that cannot be arranged on the simple cubic lattice, except if one allows for vacancies. A specific example of particular relevance for this work is archetypal pnictogen-chalcogenides of stoichiometry Pn_2Ch_3, such as As_2Se_3, that can form both a glass and a crystal. (Pn = "pnictogen," Ch = "chalcogen.") In Fig. 7 we show that coordination-wise and symmetry-wise, the structure of this compound

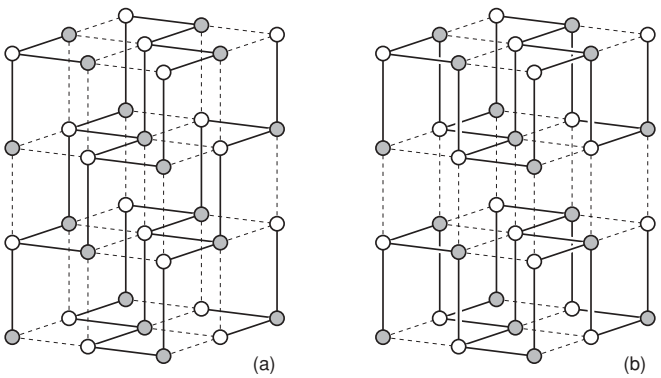

FIG. 6. Parent structure for (a) the GeTe crystal and (b) GeSe and GeS crystals, cf. Fig. 5. Note these structures are by one horizontal layer taller than the repeat unit.

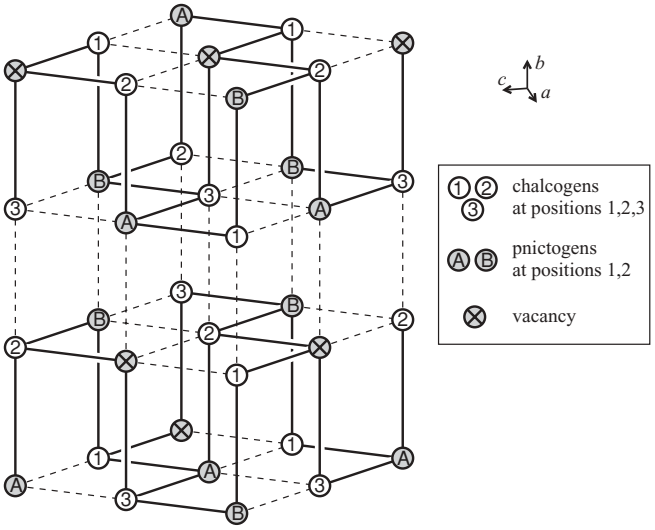

FIG. 7. A parent structure for a Pn_2Ch_3 crystal, such as crystalline As_2Se_3 and As_2S_3, c.f. Fig. 6(b).

consists of double layers similar to those in the black-phosphorus parent structure from Fig. 5(b). Note that by placing the vacancies in a particular fashion, we achieve two things simultaneously: On the one hand, the As_2Se_3 stoichiometry is obeyed, and on the other hand, the octet rule on both pnictogens and chalcogens is satisfied. In drawing individual double layers, we have used the structural model of Vanderbilt and Joannopoulos,[84] see also Ref. 85. Note that based on the actual density of As_2Se_3, the bond length in the parent structure in Fig. 7 would have to be 2.8 Å, a reasonable number consistent with the presence of the $pp\sigma$ network in the deformed structure. The presence of vacancies in parent structures should not be too surprising: The archetypal phase-change material $Ge_2Sb_2Te_5$ is known to exhibit a (metastable) distorted cubic structure with vacancies.[86,87]

The parent structure in Fig. 7 is clearly not unique in that we could have placed the double layers in several distinct positions relative to each other. The specific, "homopolar" arrangement in Fig. 7 was chosen because the sets of close neighbors in this arrangement and in the actual deformed structure seem to exhibit the greatest overlap, see Figs. 8 and 9. Nevertheless, several other mutual positions are possible, which exhibit comparably overlapping sets of close neighbors with the deformed structure, and, in addition, minimize the distance between the vacancies in the parent structure better than the specific realization in Figs. 7 and 8. For instance, consider shifting the top layer in Fig. 8 "north" by one lattice spacing. Incidentally, one notices that the vacancies in the parent structure become "smeared" in the interlayer space of the distorted structure, see Supplementary Material.[116] We point out that it would be impossible to "merge" vacancies in the Pn_2Ch_3 stoichiometry between *each* two double-layers, if we attempted to use an arseniclike structure as the parent structure from Fig. 5(a) instead of the black-phosphorus structure from Fig. 5(b). This notion is consistent with the stability of the latter structure in the actual material. At any rate, during the distortion, the distance between *linked* atoms decreases, resulting in strong, covalent bonds. Conversely, the secondary

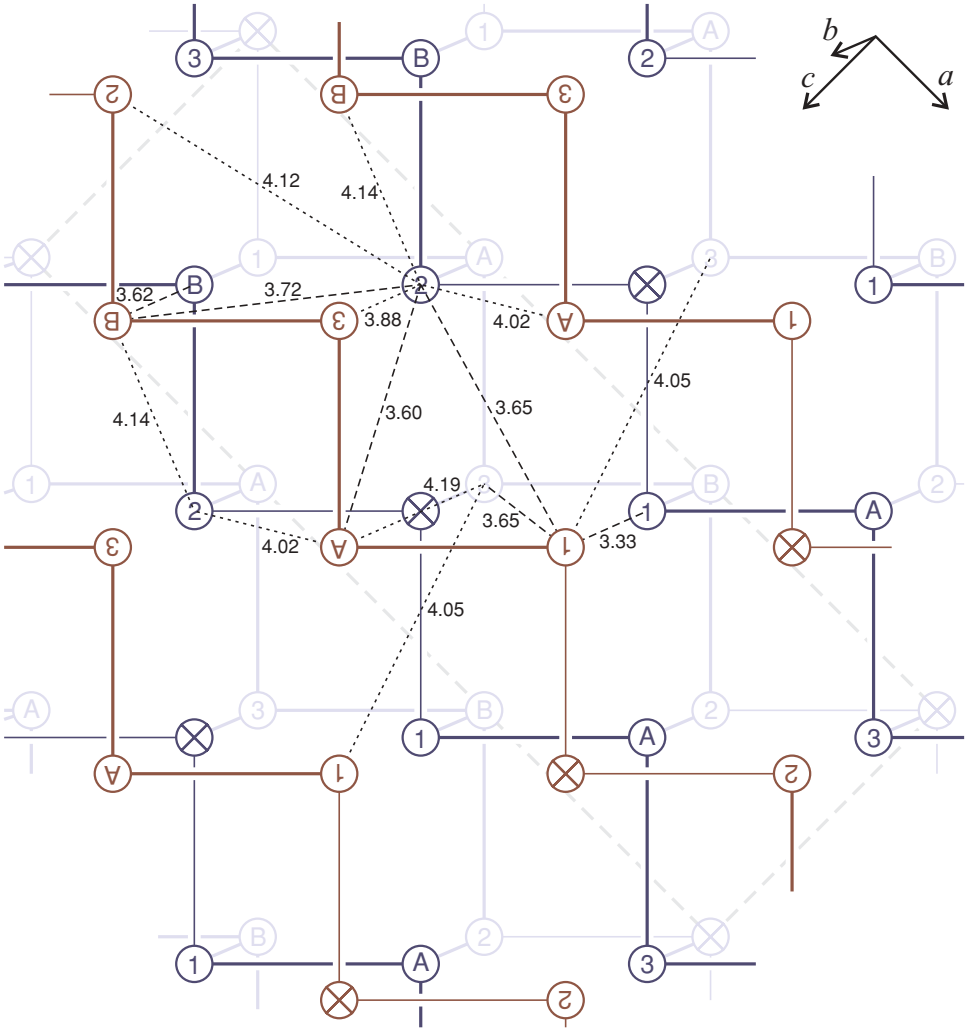

FIG. 8. The top view of a portion of the Pn_2Ch_3 parent structure from Fig. 7. The labels of the top layer are upside-down, to help distinguish it from the bottom double-layer and indicate that adjacent double layers are related by inversion. The thin dashed lines and adjacent numbers indicate the corresponding secondary bonds and their length in the deformed structure, see Fig. 9. The tilted rectangle drawn with dashed lines indicates the unit cell.

bonds will result partially from the cleaved links (usually intralayer) or new contacts that formed in the deformed structure. Figures 7–9 indicate that because the parent structure is not unique, there is no one-to-one correspondence between missing links in the parent structure and the secondary bonds in the distorted structure.

It is obvious that in the process of cleaving the bonds in the sc structure, symmetry was lowered resulting in a twice bigger unit cell along the pertinent directions. For example, in drawing the structure in Fig. 7, we could have split the original sc lattice in double-layers in six equivalent ways, i.e., two along each coordinate axis. Likewise, there are two equivalent ways to buckle each double layer, in each of the (1,1) and (1,-1) directions. Further symmetry lowering occurs when we place pnictogens, chalcogens, and vacancies at the lattice vertices. While the presence of symmetry breaking itself is hereby obvious, its mechanism appears to be subtler. Several workers have argued the symmetry-breaking transition that results in the structures of arsenic and phosphorus is Peierls-like,[25,69,77,88] which is a cooperative analog of the Jahn–Teller (JT) distortion[89] in 1D or quasi-1D solids. The precise degree of Fermi surface nesting,[90] requisite for such a structural instability, seems, however, to be subject to a specific approximation employed.[25,91] The special significance of near-*octahedral* coordination and the resulting

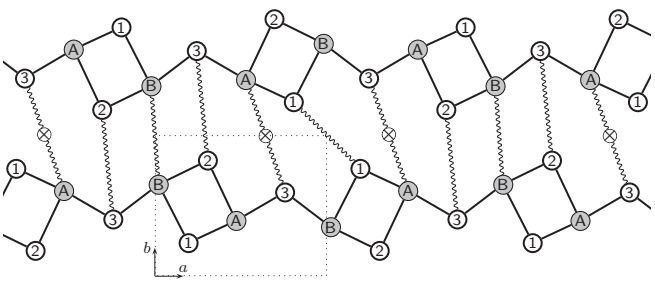

FIG. 9. A side view of the actual As_2Se_3 structure. The wavy lines indicate interlayer nearest neighbors in the parent structure, except the A-3 link, which is through a vacancy. Note that the bonded intralayer atoms are automatically nearest neighbors in the parent structure. The lengths of the links are only partially indicative of the actual bond length because the bonds are not parallel to the projection plane.

trans-influence between the corresponding covalent and secondary bonds, with regard to the Peierls metal–insulator transition, can be viewed from yet another angle: Alcock[40] points out that compounds in which the two bond types display similar length show noticeable metallic luster.

We thus conclude that one should generally regard the symmetry breaking of periodic sc parent structures as a *second*-order (or pseudo) Jahn–Teller distortion,[89] whereby strict electronic degeneracy is not required. We further note that the solid-state analogs of the second-order JT effect are also well known, such as the dimerization transition in a *hetero*polymer,[92] or in coupled homopolar chains, such as polyacene.[26] Here, the polymer chain is unstable toward dimerization so long as the gap is smaller than the coupling to the symmetry-breaking perturbation, see Eq. (2). Electronic interactions, too, can lead to an effective one-particle gap.[14] Although second-order JT symmetry breaking, whenever present, is partially hampered by the lack of degeneracy, it is still driven by the very same mechanism as during a strict Jahn–Teller–Peierls distortion.

We note that the question of the mechanism of the symmetry breaking is generally distinct from that of the interaction that determines the relaxed structure upon the symmetry breaking. According to Sec. II, the latter interaction in distorted-octahedral coordinated compounds is dominated by sp-mixing. Indeed, Seo and Hoffmann point out[91] that the distortion of the relaxed structures away from the simple cubic structure is stronger for lighter elements, consistent with stronger sp^3 hybridization in those elements. For the perturbation caused by sp-mixing to also contribute to the symmetry breaking itself, it is essential that this perturbation can be made periodic with the inverse period commensurate with the electron-filling fraction in the undistorted structure, as is the case ($1/2 = 1/2$) for trans-polyacetylene and arsenic. Otherwise, the Peierls-driven destabilization is severely weakened (Ref. 26, Chapter 2.6).

Specifically *three*-coordinated lattices with right angles between bonds have a very special property that make them additionally unstable toward symmetry lowering, even if these lattices are *aperiodic*. Any such lattice[78] can be thought of as made of linear chains, *each* of which consists of white and black segments of equal length in strict alternation. The junctions between adjacent segments correspond to the lattice vertices, while the white and black segments themselves correspond to no-link and link, respectively. In the case of strict octahedral coordination, i.e., no mixing between distinct chains, *each* such chain can be thought of as a result of a Peierls distortion of a chain of equidistant atoms. As a result, even aperiodic parent structures are expected to be relatively (meta-)stable, not only the strictly periodic structures of arsenic or black phosphorus. We illustrate the symmetry breaking in an individual linear $pp\sigma$ system in the presence of significant sp-mixing, which will be also of use later. Shown in Fig. 10 is a dimerized linear chain of hydrogen-passivated arsenics, $(AsH_2)_n$. The details of the electronic structure and geometry determination for the chain are provided in Appendix C. Despite the presence of sp-mixing and other interactions, the chain exhibits a clear $pp\sigma$-character (see Fig. 1 for the notations). The As–As bond length are $d = 2.48$ Å and $d' = 3.0$ Å for the covalent and secondary bonds, respectively. The bond angles are $\alpha_{\mathrm{HAsH}} = 97^\circ$, $\beta_{\mathrm{AsAsAs}} = 150^\circ$. The secondary bonding is significant as witnessed by the value of the corresponding transfer integral: $t' \simeq 2.3$ eV, i.e., almost a half of that for the covalent counterpart: $t \simeq 4.9$ eV. The competing interactions, i.e., ss, sp-mixing, and $pp\pi$ are significantly smaller (see Appendix C), implying the bonding is indeed $pp\sigma$. The sp-transfer integral is as large as 57% of the $pp\sigma$ transfer integral, consistent with the earlier statement that the sp-mixing is the next leading contributor to the geometry of the symmetry- broken state, after the $pp\sigma$ interaction itself. As expected of a Peierls insulator, the chain exhibits a perfect bond alternation pattern. Lastly, note that even though individual chains that make up aperiodic 3D parent structures undergo Peierls transitions, the symmetry breaking for the 3D structures themselves is generally not quasi-one dimensional and thus is not Peierls, in contrast with periodic systems, such as considered by Burdett and others.

The parent structures with three links per atom plus vacancies, if any, see Figs. 5–7, can serve as basic models for compounds with distorted octahedral coordination that consist of two- and three-valent elements. These structures also apply to compounds containing elements from group 14, such as GeTe, GeSe from Fig. 6 or archetypal phase-change alloys $Ge_2Sb_2Te_5$ and $GeSb_2Te_4$.[93] Hereby each $A^{IV}B^{VI}$ pair is isolectronic with a pair of pnictogens, implying these atoms are three-coordinated. The rest of the atoms are in the Pn_2Ch_3 stoichiometry, and so the rules leading to the parent structure in Fig. 7 apply to these atoms. Even in the absence of $A^{IV}B^{VI}$ pairing, symmetry-breaking schemes can be proposed for substances where the number of four-coordinated atoms is large, as in GeP and TlI,[80] or β-tin,[88] and similarly for five-coordinated atoms.[88] Otherwise, an atom with coordination four or higher can be considered as a defect in a lattice of three-coordinated vertices. We will return to this important point in the companion article.[20]

The following picture of structure-formation in $pp\sigma$-networked materials, thus, emerges from the above considerations: These materials may be thought of as symmetry-broken versions of a simple cubic structure. The symmetry breaking is an interplay of several types of perturbation: (a) Peierls-instability proper for extended near-linear chains; (b) cooperative second-order Jahn–Teller distortion that results from mixing of the p-orbitals with other orbitals, mostly s, and from electronic interactions; (c) steric effects due to vacancies, if the latter must be present owing to stoichiometry, as in Fig. 7; and (d) other coordination variations, as in the case of elements from groups 14 and lower. Even though these perturbations are strong enough to break the symmetry, they are still *perturbations*, so that the resulting bonding is primarily $pp\sigma$. This statement can be quantified by comparing the strengths of the corresponding transfer integrals in the deformed structure, see Table I and the $(AsH_2)_n$ example above.

Now, one must recognize that upon geometric optimization, the lattice will generally be *aperiodic*, even when the link-breaking pattern in the parent structure is itself strictly periodic, let alone if we arranged the distinct species or vacancies aperiodically or with a period incommensurate with

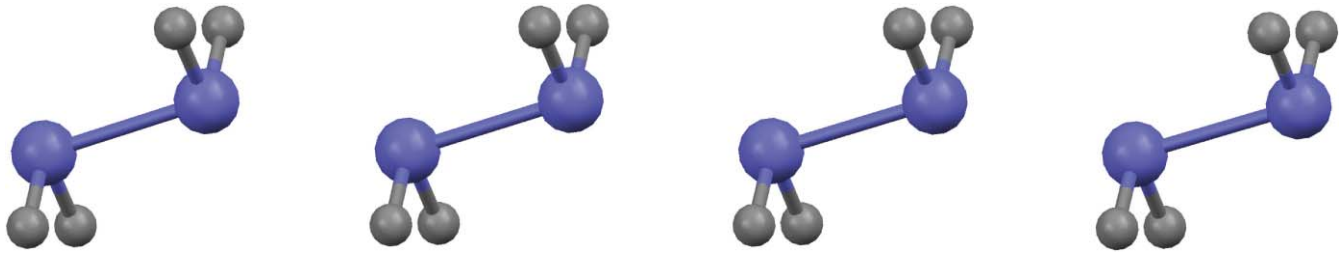

FIG. 10. The Peierls distorted $(AsH_2)_n$ chain. The links and gaps correspond to covalent bond (bond order 0.9) and secondary bonds (bond order 0.1), respectively.

the period prescribed by the electron filling fraction. Let us now examine how such aperiodic lattices maintain the $pp\sigma$ character, and hence the stability with respect to other types of ordering, while, at the same time, allowing for molecular transport.

For concreteness, let us consider a specific prescription to deform the parent sc structure. For each atom, consider the links in the parent structure as *vectors* that start on the atom. Move each atom by a small distance in the direction which is the sum of its own vectors. For instance, if an atom has three links: (1, 0, 0), (0, –1, 0), and (0, 0, –1), move it in the direction (1, –1, –1). Analogously for a two-coordinated atom, the displacement will be in the plane containing the two links. Now turn on the interaction in the form of nonzero transfer integrals, such as listed in Tables I and II. Let the lattice relax, subject of course to the Coulomb repulsion between the ionic cores. As already mentioned, there is generally no one-to-one correspondence between the parent and the distorted structure: this implies there are multiple relaxed structures and hence *multiple metastable minima on the total energy surface*. In discussing Figs. 7–9, we have mentioned that distinct parent structures for the Pn_2Ch_3 stoichiometry can be obtained by shifting the double layers relative to each other. Because such a shift incurs bond breaking, these alternative parent structures are separated by barriers. It is understood that since the parent structure is generally aperiodic,[20] Figs. 7–9 apply only to a small fragment of such an aperiodic structure. Now, since the distinct parent structures are separated by an energy barrier, at least one of them should be separated by a barrier from the actual deformed structure, implying a presence of additional, metastable minima. When such metastable minima are few, the global potential energy minimum is easily accessible, as is probably the case for the periodic parent structure of arsenic, see Fig. 5(a). Elemental arsenic is, in fact, a poor glassformer. (Other distinct three-coordinated parent structures exist,[78] but most of them are energetically costly.[79]) To summarize, the existence of distinct parent structures with shifted atoms is crucial for the present structural model to be consistent with the presence of molecular transport in $pp\sigma$-networks.

When aperiodic, the distorted lattice will exhibit two key features: first, if the substance forms a periodic crystal, it will be lower in energy than any aperiodic counterpart. Second, because aperiodic structures are not unique, the lattice will be highly degenerate, as just discussed. We can also understand the emergence of the degeneracy thermodynamically: Suppose the substance can crystallize. A mechanically stable aperiodic structure, on the one hand, has a much lower symmetry than the crystal. On the other hand, the aperiodic structure corresponds to a higher energy and hence higher *temperature*. The only way to reconcile these two conflicting notions is to recognize that there should be a thermodynamically large number of nearly degenerate aperiodic structures separated by finite barriers. By virtue of barrier crossing events, the lattice is able to restore the full translational symmetry at long enough times; the latter symmetry is higher than that in a mechanically stable crystal. The lattice, therefore, corresponds to a *liquid* in the activated transport regime, if steady state,[94] or to an aging glass, if below the glass transition.[17]

The view of quenched liquids and frozen glasses as broken symmetry phases is supported by an independent argument: According to Fig. 4, the symmetry- broken phase corresponds to a lower pressure. Bevzenko and Lubchenko[95] have shown that a covalently bonded equilibrium melt can be regarded as a high-symmetry lattice that has been sufficiently *dilated* and then allowed to relax into one of the many available aperiodic configurations. Now, are the predicted structural degeneracy of emergent aperiodic $pp\sigma$-networks and the barriers for activated reconfigurations consistent with the configurational entropy of actual materials? The contiguity between covalent and secondary bonding, as illustrated in Fig. 4, suggests that $pp\sigma$-networks support atomic motions that do not involve bond-breaking but only a gradual change in the coordination, and as such, may be thermally accessible. These special atomic motions will be discussed in detail in the follow-up article.[20]

Available structural data are consistent with the prevalence of $pp\sigma$-bonding in *vitreous* chalcogenides with the stoichiometries in question. According to several studies,[71,96] the nearest neighbor bond lengths in amorphous arsenic chalcogenides are essentially identical on the average to those in their crystalline counterparts, but have a somewhat broader distribution. In view of the argued presence of trans-influence between the covalent and secondary bonds in these compounds, we conclude that the secondary bonds in the vitreous samples are of strength comparable to those in the corresponding crystals, again subject to a broader distribution. Consequently, based on the applicability of the same general mechanism of $pp\sigma$-network formation and the comparable bonding strength, we conclude both periodic and aperiodic lattices exhibit the same type of bonding. Still, for the sake of the argument, suppose on the contrary that the bonding is dominated not by the $pp\sigma$ interaction, but by its leading

competitor, i.e., sp-mixing, thus resulting in a predominantly tetrahedral coordination. The ratio of the filling fractions of the diamond and As_2Se_3 lattices is approximately 1.18. At the same time, the densities[55,96,97] of the amorphous and crystalline compounds differ by less, i.e., is 4.57 versus 4.81–5.01 g/cm^3 for As_2Se_3 and 3.19 versus 3.46 g/cm^3 for As_2S_3, implying that only a small fraction of atoms in these glasses, if any, might be regarded as tetrahedrally coordinated. Such a "defect" is analogous to a small region occupied by an interface between two distinct lattices, which incurs a significant free energy cost. The companion article[20] shows that a mechanism for a reversible formation of such defected configurations arises naturally in the present structural model.

IV. CONCLUDING REMARKS

The main goal of this article was to establish the mechanism of bonding in semiconducting pnictogen- and chalcogen-containing quenched melts and frozen glasses. Representative substances are archetypal glassformers, such as As_2Se_3 and similar materials whose crystalline forms can be directly argued to exhibit $pp\sigma$-bonding, based on their known structures, measured electronic density of states, and electronic structure calculations. We have formulated a structural model, by which both the crystalline and vitreous materials are seen to form by the same general mechanism, i.e., by symmetry lowering and distortion of a high-symmetry structure defined on the simple cubic lattice. By combining this model with the limited structural data on the vitreous counterparts of those listed materials and similar compounds, we have argued the glasses are also $pp\sigma$-bonded.

Lowering of the symmetry by breaking the bonds in the fully connected simple cubic structure can be understood as lowering of the lattice dimensionality, similarly to what is seen in the $(AsH_2)_n$ chain in Fig. 10, which is a linear array of relatively weakly bonded dimers, or to what one finds in the parent structures from Figs. 5–7, which consist of double-layers, possibly accompanied by further symmetry lowering. Papoian and Hoffmann[43] have outlined general principles for the interrelation of dimensionality and deformation of high-symmetry periodic structures. These authors argue the bonding in the parent structures from Fig. 5 can be regarded as a Peierls distortion of a hypervalently bonded lattice built from electron-rich units, whereby the dimensionality of the lattice is lowered. In contrast, to *preserve* the dimensionality, the electron-rich units comprising the hypervalent structure would have to be oxidized instead. In the former case, the deformed structure retains its original character, while in the latter case, the geometry is expected to change. For instance, a cubic Sb^0 lattice exhibits a (distorted) octahedral coordination, while oxidation would hypothetically result in a tetrahedrally coordinated Sb^+ lattice. The semiconducting alloys in question do exhibit relatively low variation in electronegativity and, hence, the distorted octahedral coordination.

The parent structures for substances at the focus of the present study, i.e., pnictogen and chalcogen-containing alloys enjoy a very special property: Each vertex in the parent structure is *three*-coordinated, while the bonds are at near 90° angles. Under these special circumstances, the whole lattice can be thought of as composed of infinite linear chains in which bond and bond-gaps strictly alternate. In view of the weak interaction with the environment, each of these chains can be thought of as a quasi-1D Peierls insulator with renormalized interactions. (In the eventual deformed structure, the chains are deformed and, likely, of rather limited length.[20]) This observation allows one to extend the trends established by Papoian and Hoffmann in periodic crystals to *aperiodic* lattices. Since the symmetry can be restored partially or fully by high pressure, the argued view of glasses as lowered-symmetry versions of high-symmetry structures is supported by independent arguments on (negative) pressure-driven glass transition in covalently bonded materials.[95] We have also pointed out that the view of this type of symmetry breaking as a second order, cooperative Jahn–Teller distortion may be equally justified. In addition to the Peierls instability proper, within each chain, the symmetry breaking is also driven by local interactions that compete with the $pp\sigma$-bonding proper, primarily by the sp-mixing.

The presence of competing interactions in these glass-forming materials is consistent with their structural degeneracy.[98] It appears that the strength of such competing interactions should satisfy certain restrictions. Specifically, if the sp-mixing is too strong, it destroys the $pp\sigma$-bonding. Yet, if the mixing is sufficiently weak, the coordination can be made close to perfect octahedral while decreasing the stability of the glass relative to the crystal. The latter trend is exploited in making optical drives, using $Ge_2Sb_2Te_5$ or similar compounds.[86,87] Again consistent with the structural degeneracy of the $pp\sigma$-networks is the noted analogy between the bond-placement rules in the proposed structural model and the vertex models known to exhibit rich phase behavior.[83,99]

The argued similarity of the bonding mechanisms in $pp\sigma$-bonded crystals and glasses explains the puzzling stability of this important class of glasses. As mentioned in the Introduction, the enthalpy excess ΔH of the supercooled liquid, relative to the corresponding crystal, is easy to estimate. It is directly related to the configurational entropy S_c of the fluid, i.e., $\Delta H = S_c T$, save a small ambiguity stemming from possible differences in the vibrational entropies. The liquid configurational entropy varies between $0.8k_B$ and about $2k_B$ per bead, between the glass transition[16] and melting temperatures. The energy $0.8k_B T_g$ per bead amounts to less than 0.05 eV per atom. The model, thus, allows one to reconcile two seemingly conflicting characteristics of quenched melts and frozen glasses. On the one hand, these materials exhibit remarkable thermodynamic and mechanical stability, only slightly inferior to the corresponding crystals. On the other hand, these materials are also multiply degenerate thus allowing for molecular transport.

Finally, this paper buttresses and clarifies some of the technical aspects of the original programme: The $pp\sigma$-networks automatically satisfy all the necessary requirements for the presence of the intrinsic midgap electronic states, as listed in the Introduction. First, a necessary requirement for covalent $pp\sigma$ bonding is that the electronegativity variation ϵ is not too large, Eq. (2), lest the resulting bonding becomes predominantly ionic. Second, a high

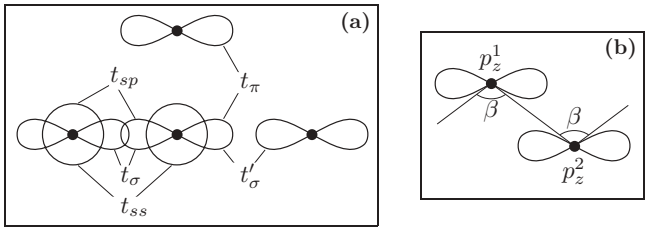

FIG. 11. (a) A graphical summary of the definitions of the transfer integrals from Table I. (b) An example of geometry used to compute transfer integrals t and t', see text.

symmetry $pp\sigma$-bonded network is unstable toward Jahn–Teller distortion at each center, implying the deformed lattice shows an alternating pattern of bond saturation in the form of covalent and secondary bonds. Third, based on the stability of the $pp\sigma$-network with respect to perturbations in the form of competing chemical interaction, the secondary bonds are sufficiently strong, i.e., the t'/t ratio of the transfer integral of the secondary and covalent bonds is not too small, see Eq. (1).

ACKNOWLEDGMENTS

The authors thank David M. Hoffman, Thomas A. Albright, Peter G. Wolynes, and the anonymous Reviewer for helpful suggestions. We gratefully acknowledge the Arnold and Mabel Beckman Foundation Beckman Young Investigator Award, the Donors of the American Chemical Society Petroleum Research Fund, and NSF Grant No. CHE-0956127 for partial support of this research.

APPENDIX A: DETAILED EXPLANATIONS OF TABLES I AND II

Table I: A graphical summary of the definitions of the transfer integrals is given in Fig. 11(a), see also p. 23 of Ref. 37. By definition, the $pp\sigma$ integrals, i.e., t_σ and t'_σ are computed assuming the two p orbitals are aligned with the bond and hence depend only on the distance between the participating atoms. As a result, the transfer integrals t and t' from Eq. (1) are equal in value to t_σ and t'_σ, respectively only when the three atoms in question are situated on a straight line. If $180 - \beta < 20^\circ$, as is the case for almost all compounds from Table I, the difference between t and t_σ is less than a few percent, depending on the specific geometry and basis set. For instance, in the geometry from Fig. 11(b), we get $t = \langle p_z^1 | \mathcal{H} | p_z^2 \rangle = t_\sigma + (t_\pi - t_\sigma)\cos^2(\beta/2)$, yielding a difference of 4% between t and t_σ for $\beta = 160^\circ$ and $t_\pi/t_\sigma = -1/4$, Ref. 48.

Table II: For several compounds, the structural data vary somewhat depending on the source, such as for As_4Se_4 in Refs. 56 and 100 and α-monoclinic Se, Refs. 59 and 64 The resulting ambiguity should be kept in mind.

2nd column, deviation from the right-angled geometry. For As_2O_3, $GeSe_2$, and $AsBr_3$ only As and Ge were considered as the central atoms.

3rd column. The absolute electronegativity is the average of the electron ionization and affinity energies, as found in Ref. 101.

TABLE III. Covalent radii. The three columns contain the species name, the reference structure, and the resulting radius.

	Reference structure	r_{cov} (Å)
O	α-quartz-GeO_2 crystal	0.52
Ge	Crystal	1.225
As	See text	1.20
Se	Isolated helix (105) and rings	1.17
Br	Diatomic molecule	1.140
Te	Isolated helix and rings (106)	1.37

4th, 5th column. The covalent radii used are listed in Table III. These radii were determined using compounds exhibiting low variations in electronegativity, as pertinent to the materials in question, except GeO_2. For As, values found in the literature[102–104] differ within 0.02 Å. We use the value from the middle of this range, which also happens to coincide with the result of interpolation across the sequence of Ge-As-Se-Br.

6th column. Only the strongest secondary bonds are cited. To determine these for As_4Se_4 and Se, we have used diagrams that show the magnitudes of the atomic p orbitals of the nearby atoms on a sphere centered on a chosen atom with a radius equal to the covalent radius of that atom, see the Supplementary Material.[116] For the tetrahedrally bonded materials, As_2O_3, and $AsBr_3$, the nearest neighbor in the direction opposite to the covalent bonded atoms is used.

7th column. Accurate values of the tight-binding parameters are usually determined by obtaining the best fit to the electronic density of states for each specific systems and are thus system-dependent. Our goal here is, instead, to highlight the *generic* trends of tight-binding parameters that apply satisfactorily for bonds ranging from the strictly covalent to van der Waals, in as many distinct compounds as possible. Such a universal parametrization of one-electron transfer (resonance) integrals is provided, for instance, by the PM6 parametrization[107] of the MNDO method,[108] which we use to estimate the t'_σ/t_σ ratios for the compounds in Table II. Despite the made approximations, we feel that the resulting potential ambiguity of the *ratio* of the matrix elements, t'_σ/t_σ, is not large.

We can partially judge the reliability of the tight-binding parameters by comparing them to those obtained by other standard methods. In Table IV, we compare Robertson's data[39] for transfer integrals in three elemental solids, as obtained by fitting the spectrum of the one-electron TB Hamiltonian (column 2) and by the chemical pseudopotential method (column 3) to the present TB parametrization (column 4). The

TABLE IV. Comparison of the t'_σ/t_σ ratio, as resulting from the present tight-binding parametrization with compilations of Robertson (Ref. 39) (table) and the calculations of Bernstein *et al.* (Ref. 109) (figure), see text.

	Ref. 39 TB fit	Ref. 39 pseud.	Present work
As	0.54	0.51	0.62
Se	0.19	0.26	0.27
Te	0.33	0.65	0.74

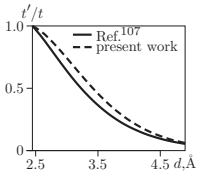

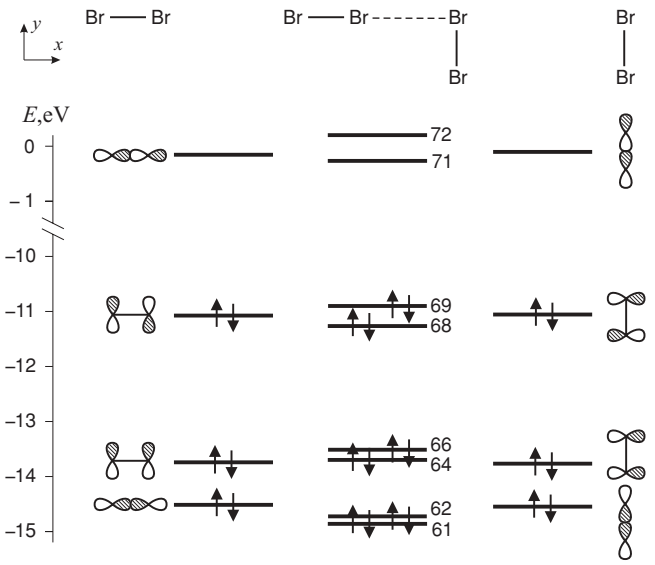

FIG. 12. MO diagram of the Br_2 dimer from Fig. 3 that depicts a subset of the MO's from Table V, along with pertinent MO's of the constituent Br_2 molecules.

figure on the rhs compares the result of the parametrization for elemental Ge with accurate calculations of Bernstein *et al.*[109] Finally, the same TB parametrization was used for calculation on the dimer of Br_2 molecules, see below.

APPENDIX B: DIMER OF BROMINE MOLECULES

In this appendix, we use the electronic structure of Br_2–Br_2 dimer obtained by *ab initio* calculations to estimate the contribution of the $pp\sigma$ interaction to the binding energy of the dimer and show that the resulting estimate is consistent with the conclusions of a simple molecular orbital theory.

The geometry of the dimer (see Fig. 3) is optimized by FIREFLY(Ref. 67) program on MP2-level with aug-cc-pVTZ basis set and RHF (Restricted Hartree-Fock) wavefunction. Although more accurate approximations exist,[110] the present method has the advantage of simplicity while yielding the geometry consistent with that of the bromine crystal; it also yields results that compare well with accurate calculations for other halogen dimers.[111] For clarity, we have not corrected for the basis set superposition error, because here we are interested in the relative magnitudes of distinct contributions to the bonding, not the absolute value of the binding energy. The resulting ambiguity in the binding energy itself is not large anyway, about 15%, as can be estimated using the standard counterpoise method, Ref. 112, p. 714.

The total binding energy of the dimer, 0.13 eV, consists of several contributions. For instance, the correlation (MP2) contribution is 0.2 eV. To extract the contribution proper of the electrons occupying distinct molecular orbitals, we adhere to the following scheme: First, we subtract the uniform downshift of all MOs by 20 meV in the dimer, relative to the two isolated Br_2 molecules. Next, we compile the contributions of all molecular orbitals to the bonding, see Table V. Here, the dimer is in the x-y plane. Because little sp-mixing is present, the MO's are naturally grouped into classes that consist primarily of either p or s orbitals. The p orbitals are further subdivided, according to their symmetry, into $p_{x,y}$ and p_z orbitals. The former form the $pp\sigma$ bonds, while the latter are out of the x–y plane and contribute little to the bonding, as is clear from Table V.

The magnitude of the binding energy due to the in-plane p-orbitals, 0.284 eV, can be rationalized using a simple molecular orbital theory. Let us first consider only the eight valence p-orbitals lying in the plane of the dimer shown in Fig. 3. The *ab initio* diagram of the corresponding MO's is shown in Fig. 12. Let us focus exclusively on the intramolecular $pp\sigma$- and $pp\pi$-interactions and the intermolecular $pp\sigma$-interaction between two atoms connected by the dashed line in Fig. 3. In this approximation, the p_y orbitals do not interact with the p_x orbitals, so that the secondary bonding is exclusively due to the p_x orbitals. The specific realization of Hamiltonian (3) for this bonding configuration reads

$$\mathcal{H} = \begin{pmatrix} \epsilon_p & t_\sigma & 0 & 0 \\ t_\sigma & \epsilon_p & t'_\sigma & 0 \\ 0 & t'_\sigma & \epsilon_p & t_\pi \\ 0 & 0 & t_\pi & \epsilon_p \end{pmatrix}. \tag{B1}$$

By Eq. (4), combined with

$$E^{\mathrm{A}}_{\mathrm{unocc}} = \epsilon_p + t_\sigma, \quad \psi^{\mathrm{A}}_{\mathrm{unocc}} = \frac{1}{\sqrt{2}}\begin{pmatrix}1\\1\end{pmatrix},$$

$$E^{\mathrm{B}}_{\mathrm{occ}} = \epsilon_p \pm t_\pi, \quad \psi^{\mathrm{B}}_{\mathrm{occ}} = \frac{1}{\sqrt{2}}\begin{pmatrix}1\\\pm 1\end{pmatrix},$$

we obtain the dimer binding energy

$$(t'_\sigma)^2/t_\sigma. \tag{B2}$$

Generally, in the perturbative expression (4), the quantities V_{nm} correspond to the transfer integrals of the secondary bonds, t', while the denominators to the transfer integrals of the covalent bonds, t. The binding energy is, thus, second order in the t'/t ratio.

Note that the result in Eq. (B2) also helps to partially assess the reliability of the TB parametrization from Appendix A. Substituting the numerical values for those transfer integrals in Eq. (B2) yields the dimer bonding energy 0.3 eV, in good agreement with the *ab initio* analysis leading to Table V. A similar analysis can be used to show that the s-orbital bonding contribution from Table V results not from the ss interaction, but primarily from sp-mixing, also consistent with the small overlap of the s-orbitals.

Finally, we outline derivation of the TB expression (5) for the bond order of a closed-shell interaction. Using Eq. (14.22)

TABLE V. Bonding contribution of the molecular orbitals (MOs) of the Br_2–Br_2 dimer from Fig. 3. The quantity E_{binding} is the difference between the total MO energies of the dimer and those of the isolated molecules.

MOs	AOs	Energy range, eV	E_{binding}, eV
61, 62, 64, 66, 68, 69	$p_{x,y}$	(−14.90, −10.9)	−0.284
57, 58, 59, 60	s	(−30.3, −25.7)	−0.195
63, 65, 67, 70	p_z	(−14.0, −10.9)	−0.075
71, 72 (unocc.)	s, $p_{x,y}$	(−0.3, +0.2)	+0.466

TABLE VI. The geometry of the dimer of As_2H_4 molecules: semiempirical PM6 calculations, *ab initio* RHF MP2 calculations with acc-pVDZ basis set, and calculations from Ref. 115 The notations are according to Fig. 1, two entries per cell correspond to the inner (1st) and the outer (2nd) AsH_2 units, the energy is the dimer binding energy, the values in parentheses are not optimized.

	d_{AsAs}	d'_{AsAs}	β	d_{AsH}	α_{HAsH}	α_{AsAsH}	E (eV)
PM6	2.463	3.06	148	1.523	95.7	97.4	−0.17
				1.523	95.6	96.9	
MP2	2.483	3.57	177	1.525	91.7	92.6	−0.13
				1.527	91.6	92.1	
Ref. 115	(2.441)	3.53	(180)	(1.506)	(93.9)	(93.9)	−0.10

of Ref. 47, for the wave-functions of an AB dimer formed by a closed- shell interaction, one can straightforwardly show that the interaction-induced correction to the density matrix $\mathcal{P}$ for the dimer, in the second order, is given by

$$\left\{\sum_n^{A_{occ}}\sum_m^{B_{unocc}} - \sum_n^{A_{unocc}}\sum_m^{B_{occ}}\right\}\frac{V_{nm}}{E_n^A - E_m^B} \times \begin{pmatrix} 0 & |\psi_n^A\rangle\langle\psi_m^B| \\ |\psi_m^B\rangle\langle\psi_n^A| & 0 \end{pmatrix}. \tag{B3}$$

According to a standard definition of the bond order,[65] (also used in MOPAC), the latter can be written in the chosen basis set as

$$b_{AB} = \sum_n^A\sum_m^B \left|(\langle\psi_n^A|, 0)\mathcal{P}\begin{pmatrix}0\\|\psi_m^B\rangle\end{pmatrix}\right|^2, \tag{B4}$$

leading to Eq. (5).

Note that the first (second) double sum in Eq. (5) is twice the occupation of the antibonding orbitals of the molecule B (A), as donated by the bonding orbitals of A (B). These occupations are defined as $2\sum_\nu^{(AB)_{occ}}\sum_m^{B_{unocc}}|\langle\psi_m^B|\psi_\nu\rangle|^2$ and $2\sum_\nu^{(AB)_{occ}}\sum_m^{A_{unocc}}|\langle\psi_m^A|\psi_\nu\rangle|^2$, respectively, where ψ_ν are MO's of the AB dimer.

APPENDIX C: ARSENIC CHAIN

In our model system, the dimerized $(AsH_2)_n$ chain (Fig. 10), the shorter and longer As–As bonds correspond to covalent and secondary bonds, respectively; the As–H bonds correspond to covalent bonds in chalcogenide glasses. The calculations are performed on semiempirical level by MOPAC[113] program with PM6 parametrization. On each arsenic, the axes are labelled as follows: The p_x and p_y orbitals are oriented toward the hydrogens (but not strictly along the x and y axis), while p_z orbitals are directed toward the neighboring arsenics, see the geometry in Fig. 11(b). Note these axes are defined locally on each individual arsenic; the optimized chain may or may not be linear on the average.

We first check the semiempirical approximation against *ab initio* calculations for $n = 4$, see Table VI. The *ab initio* results clearly indicate a distorted octahedral geometry and are consistent with secondary bonding between the terminal $(AsH_2)_2$ units: The β (As–As–As) angle is very close to 180°, while the bond length, 3.57 Å, is close but shorter than the sum of the reported van der Waals radii for As, i.e., between 3.7 and 3.9 Å, depending on the convention.[114] Now, judging from the angle β between adjacent As–As bonds and H-As-H angle, the semiempirical method clearly overestimates the tendency toward sp^3 hybridization. At the same time, the semiempirical method underestimates the secondary bond length, suggesting the two errors in the resulting bond strength will partially cancel out. The discrepancy in the secondary bond lengths and the β angles between the *ab initio* and PM6 methods should be considered a consequence of the specific parametrization adopted in MOPAC, which was optimized for covalent, not secondary bonds, and many of which have a significant ionic component and/or coordinations distinct from distorted octahedral. Thus the TB-based analysis is not expected to be fully quantitative, unless *ad hoc* parametrized. Nevertheless, we have seen from the discussion of Eqs. (4) and (5) that TB analysis is qualitatively consistent with the closed-shell character of the secondary bonding and the trans-influence between the counterpart covalent and secondary bonds. Our results for geometric optimization of rhombohedral arsenic, using the PM6 parametrization, are consistent with these conclusions: Using a 96 atom supercell, we obtain $d = 2.46$ Å (versus experimental 2.52 Å), $d' = 3.24$ Å (3.10 Å), $\alpha = 99.3°$ (96.7°). Clearly, the PM6 parametrization is consistent with $pp\sigma$ bonding in rhombohedral As, and, furthermore, gives reasonable figures for the lattice parameters.

According to the semiempirical calculation, an *infinite* AsH_2 chain is dimerized and has a zero net curvature, whereby $d = 2.48$ Å, $d' = 3.0$ Å, $\alpha = 97°$, $\beta = 150°$. Despite the aforementioned bias toward sp-mixing, analysis of localized MOs in the semiempirical calculations shows that the bonding contribution of arsenic's s-orbitals is negligible: 0.1 (versus 2 for a regular bond). Significant secondary bonding and the trans-influence between the covalent secondary bonds are clearly seen in the values of the bond order, which are equal to 0.9 and 0.1 for the covalent and secondary As–As bond, respectively.

To independently verify the dominant character of the $pp\sigma$-bonding, we demonstrate that the competing interactions are perturbations that mostly amount to a renormalization of the $pp\sigma$-interaction. Indeed, the full *one*-particle Hamiltonian for a system plus the environment is a block matrix

$$\mathcal{H} = \begin{pmatrix} \mathcal{H}_{sys} & \mathcal{V}^\dagger \\ \mathcal{V} & \mathcal{H}_{env} \end{pmatrix}, \tag{C1}$$

where the matrix $\mathcal{H}_{sys}$ contains exclusively the on-site energies and transfer integrals for the system, $\mathcal{H}_{env}$ for the environment. The (generally nonsquare) matrix $\mathcal{V}$ and its hermitian conjugate $\mathcal{V}^\dagger$ contain the system-environment transfer integrals. It is straightforward to show that, given an energy eigenvalue E for the full Hamiltonian in Eq. (C1), the portion of the wave-function corresponding to the system is an eigenfunction of the effective Hamiltonian:

$$\tilde{\mathcal{H}} = \mathcal{H}_{sys} + \mathcal{V}^\dagger(E - \mathcal{H}_{env})^{-1}\mathcal{V} \tag{C2}$$

TABLE VII. Columns 2–5: Elements $\langle\phi|H|\psi\rangle$ of the Fock matrix of an infinite $(AsH_2)_n$ chain. The transfer integrals t and t' are indicated in brackets next to their numerical values. Column 6: The renormalization of the parameters of the one-particle $pp\sigma$-only Hamiltonian, as computed using Eq. (C2). Column 7: The contribution to this renormalization of the s-orbitals. Labels "cb" and "sb" mean covalent and secondary bonds. All AO's belong to the arsenics except the hydrogen's s_H.

$\phi \setminus \psi$	p_z	s	p_x	s_H	Renormalization	sp
p_z	−4.9	−0.6	0.2	0.1	$\tilde{\epsilon}-\epsilon=+1.2$ eV	60%
s		−13.	0.9	−4.0		
p_x			−4.4	−7.6		
s_H				−5.0		
p_z^{cb}	4.9(t)	2.8	−0.8	0.6	$\tilde{t}-t=+0.7$ eV	50%
s^{cb}		−0.7	0.4	−0.1		
p_x^{cb}			1.3	0.4		
p_z^{sb}	2.3(t')	−1.0	0.7	−0.2	$\tilde{t}'-t'=-0.3$eV	35%
s^{sb}		0.0	0.2	−0.1		
p_x^{sb}			0.5	0.2		

with the same eigenvalue E. Indeed, substituting $|\psi\rangle = (\langle\psi_{sys}|, \langle\psi_{env}|)^\dagger$ into $\mathcal{H}|\psi\rangle = E|\psi\rangle$, one gets $\mathcal{H}_{sys}|\psi_{sys}\rangle + \mathcal{V}^\dagger|\psi_{env}\rangle = E|\psi_{sys}\rangle$ and $(\mathcal{H}_{env}-E)|\psi_{env}\rangle = -\mathcal{V}|\psi_{sys}\rangle$, from which Eq. (C2) follows.

Clearly, in the one-particle picture, the effect of the environment can be presented as an (energy-dependent) renormalization of the bare Hamiltonian of the system proper. One can use this systematic procedure to estimate the strength of both the intrachain and environment's perturbation to the $pp\sigma-$ bonding within the chain. In doing so, below, we fix the energy E at the gap center.

The contribution of s or d orbitals to the renormalization of the $pp\sigma$ transfer integrals can be estimated by using a perturbative expansion of the exact Eq. (C2):

$$\tilde{\mathcal{H}}_{ij} = \mathcal{H}_{sys,ij} + \sum_\alpha \frac{t_{i\alpha}t_{\alpha j}}{E-\epsilon_\alpha} - \sum_{\alpha\beta} \frac{t_{i\alpha}t_{\alpha\beta}t_{\beta j}}{(E-\epsilon_\alpha)(E-\epsilon_\beta)} + \cdots, \quad \text{(C3)}$$

where the Latin indices label intrachain p_z orbitals and the Greek indexes label the rest of the orbitals. The small parameter $t/(E-\epsilon)$ is indeed small, and the more so the further the orbital energy ϵ from the gap center.

The essential elements of the Fock matrix are listed in Table VII. Note that d-orbitals are also included in PM6 parametrization. Despite the large value of the pertinent transfer integrals, the direct contribution of these orbitals to the renormalization is at most a few percent because the orbitals are almost empty. One infers from Table VII that the dominant contribution to As–As bonding stems from $pp\sigma$-integrals. The $pp\pi$-integrals are four times smaller than $pp\sigma$, while the ss-integrals are essentially negligible. Although s-orbitals do not by themselves contribute significantly to the bonding in the chain, they provide the main contribution to the renormalization of the $pp\sigma$ transfer integrals, specifically by *weakening* the secondary bonding. This contribution, provided in the last column in Table VII, turns out to be well approximated by the expressions:

$$\Delta\epsilon \approx -t_{sp}^2/\epsilon_s, \quad \Delta t \approx 2t_{sp}t_{sp}^{\text{on-atom}}/\epsilon_s, \quad \text{(C4)}$$

within the error of 20% or less compared with the more accurate Eq. (C3). Here

$$t_{sp}^{\text{on-atom}} \approx -g_{sp}P_{sp}/2, \quad \text{(C5)}$$

where g_{sp} is the Coulomb integral for s and p orbitals of the same atom (6 eV for As) and P_{sp} is the corresponding entry of the density matrix, which is the measure of actual hybridization. If $P_{sp} > 0$—as is the case for AsH_2 chain—then the sp-mixing weakens the secondary bonding, the magnitude of the effect proportional to the hybridization strength.

[1] K. Morigaki, *Physics of Amorphous Semiconductors* (World Scientific, Singapore, 1999).
[2] R. Zallen, *The Physics of Amorphous Solids* (Wiley, New York, 1998).
[3] A. Feltz, *Amorphous Inorganic Materials and Glasses* (Wiley, New York, 1993).
[4] S. R. Elliott, *Physics of Amorphous Materials* (Longmans, Green, New York, 1990).
[5] M. Wuttig and N. Yamada, Nature Mater. **6**, 824 (2007).
[6] D. Lencer, M. Salinga, B. Grabowski, T. Hickel, J. Neugebauer, and M. Wuttig, Nature Mater. **7**, 972 (2008).
[7] P. W. Anderson, Phys. Rev. **109**, 1492 (1958).
[8] N. Mott, Proc. R. Soc. London, Ser. A **382**, 1 (1982).
[9] M. H. Cohen, H. Fritzsche, and S. R. Ovshinsky, Phys. Rev. Lett. **22**, 1065 (1969).
[10] N. F. Mott, *Metal-Insulator Transitions* (Taylor & Francis, London, 1990).
[11] P. W. Anderson, Nature (London), Phys. Sci. **235**, 163 (1972).
[12] P. W. Anderson, Phys. Rev. Lett. **34**, 953 (1975).
[13] N. F. Mott, Rev. Mod. Phys. **50**, 203 (1978).
[14] A. Zhugayevych and V. Lubchenko, J. Chem. Phys. **132**, 044508 (2010).
[15] T. R. Kirkpatrick, D. Thirumalai, and P. G. Wolynes, Phys. Rev. A **40**, 1045 (1989).
[16] X. Xia and P. G. Wolynes, Proc. Natl. Acad. Sci. U.S.A. **97**, 2990 (2000).
[17] V. Lubchenko and P. G. Wolynes, J. Chem. Phys. **121**, 2852 (2004).
[18] V. Lubchenko and P. G. Wolynes, Annu. Rev. Phys. Chem. **58**, 235 (2007).
[19] A. J. Heeger, S. Kivelson, J. R. Schrieffer, and W. P. Su, Rev. Mod. Phys. **60**, 781 (1988).
[20] A. Zhugayevych and V. Lubchenko, J. Chem. Phys. **133**, 234504 (2010).
[21] D. K. Biegelsen and R. A. Street, Phys. Rev. Lett. **44**, 803 (1980).
[22] J. Hautala, W. D. Ohlsen, and P. C. Taylor, Phys. Rev. B **38**, 11048 (1988).
[23] T. Tada and T. Ninomiya, J. Sol. St. Comm. **71**, 247 (1989).
[24] T. N. Claytor and R. J. Sladek, Phys. Rev. Lett. **42**, 1482 (1979).
[25] S. Shang, Y. Wang, H. Zhang, and Z.-K. Liu, Phys. Rev. B **76**, 052301 (2007).
[26] J. K. Burdett, *Chemical Bonding in Solids* (Oxford University Press, New York, 1995).
[27] M. A. Popescu, Non-crystalline Chalcogenides (Kluwer, New York, 2000).
[28] J. Li and D. A. Drabold, Phys. Rev. B **61**, 11998 (2000).
[29] M. Cobb, D. A. Drabold, and R. L. Cappelletti, Phys. Rev. B **54**, 12162 (1996).
[30] S. G. Bishop, U. Strom, and P. C. Taylor, Phys. Rev. B **15**, 2278 (1977).
[31] F. Mollot, J. Cernogora, and C. Benoit à la Guillaume, Philos. Mag. B **42**, 643 (1980).
[32] P. S. Salmon, J. Non-Cryst. Solids **353**, 2959 (2007).
[33] K. Hachiya, J. Non-Cryst. Solids **291**, 160 (2001).
[34] L. Makinistian and E. A. Albanesi, J. Phys. Condens. Matter **19**, 186211 (2007).
[35] R. Azoulay, H. Thibierge, and A. Brenac, J. Non-Cryst. Solids **18**, 33 (1975).
[36] W. B. Pearson, *The Crystal Chemistry and Physics of Metals and Alloys* (Wiley, New York, 1972).
[37] W. A. Harrison, *Electronic Structure and the Properties of Solids* (Freeman, San Francisco, 1980).
[38] G. N. Greaves, S. R. Elliott, and E. A. Davis, Adv. Phys. **28**, 49 (1979).
[39] J. Robertson, Adv. Phys. **32**, 361 (1983).
[40] N. Alcock, Adv. Inorg. Chem. Radiochem. **15**, 1 (1972).
[41] P. Pyykkö, Chem. Rev. **97**, 597 (1997).
[42] G. A. Landrum and R. Hoffmann, Angew. Chem., Int. Ed. **37**, 1887 (1998).

[43]G. A. Papoian and R. Hoffmann, Angew. Chem., Int. Ed. **39**, 2408 (2000).
[44]H. A. Bent, Chem. Rev. **68**, 587 (1968).
[45]A. Antonelli, E. Tarnow, and J. D. Joannopoulos, Phys. Rev. B **33**, 2968 (1986).
[46]J. K. Burdett, Chem. Soc. Rev. **23**, 299 (1994).
[47]J. N. Murrell, S. F. A. Kettle, and J. M. Tedder, *The Chemical Bond*, 2nd ed. (Wiley, New York, 1985).
[48]W. Harrison, *Elementary Electronic Structure* (WSPC, Singapore, 2004).
[49]S. G. Bishop and N. J. Shevchik, Phys. Rev. B **12**, 1567 (1975).
[50]A. C. Stergiou and P. J. Rentzeperis, Z. Kristallogr. **172**, 139 (1985).
[51]D. Schiferl and C. S. Barrett, J. Appl. Cryst. **2**, 30 (1969).
[52]P. M. Smith, A. J. Leadbetter, and A. J. Apling, Philos. Mag. **31**, 57 (1974).
[53]H. Wiedemeier and H. G. von Schnering, Z. Kristallogr. **148**, 295 (1978).
[54]R. Keller, W. B. Holzapfel, and H. Schulz, Phys. Rev. B **16**, 4404 (1977).
[55]A. C. Stergiou and P. J. Rentzeperis, Z. Kristallogr. **173**, 185 (1985).
[56]A. L. Renninger and B. L. Averbach, Acta Crystallogr. B **29**, 1583 (1973).
[57]Y. Miyamoto, Jpn. J. Appl. Phys. **19**, 1813 (1980).
[58]B. M. Powell, K. M. Heal, and B. H. Torrie, Mol. Phys. **53**, 929 (1984).
[59]P. Cherin and P. Unger, Acta Cryst. B **28**, 313 (1972).
[60]F. Pertlik, Monatsch. Chemie **109**, 277 (1978).
[61]H. Braekken, Forh. - K. Nor. Vidensk. Selsk. **8**, 3 (1935).
[62]G. von Dittmar and H. Schafer, Acta Crystallogr. B **32**, 2726 (1976).
[63]Y. Zhang, Z. Iqbal, S. Vijayalakshmi, S. Qadri, and H. Grebel, J. Sol. State Comm. **115**, 657 (2000).
[64]R. W. G. Wyckoff, *Crystal Structures* (Interscience, New York, 1963).
[65]D. R. Armstrong, P. G. Perkins, and J. J. P. Stewart, J. Chem. Soc. Dalton Trans. **838**, 1973 (1973).
[66]A. A. Granovsky, Firefly version 7.1.G, http://classic.chem.msu.su/gran/firefly/index.html.
[67]W. P. Anderson, J. K. Burdett, and P. T. Czech, J. Amer. Chem. Soc. **116**, 8808 (1994).
[68]P. Silas, J. R. Yates, and P. D. Haynes, Phys. Rev. B **78**, 174101 (2008).
[69]R. Bellissent, C. Bergman, R. Ceolin, and J. P. Gaspard, Phys. Rev. Lett. **59**, 661 (1987).
[70]R. Bellissent and G. Tourand, J. Non-Cryst. Solids **35**, 1221 (1980).
[71]S. Hosokawa, A. Goldbach, M. Boll, and F. Hensel, Phys. Stat. Sol. (b) **215**, 785 (1999).
[72]R. Zallen, R. E. Drews, R. L. Emerald, and M. L. Slade, Phys. Rev. Lett. **26**, 1564 (1971).
[73]L. M. Falicov and S. Golin, Phys. Rev. **137**, A871 (1965).
[74]M. Takumi and K. Nagata, J. Phys. Soc. Jpn. **76**, 17 (2007).
[75]H. Fujihisa, Y. Fujii, K. Takemura, and O. Shimomura, J. Phys. Chem. Solids **56**, 1439 (1995).
[76]H. Katzke and P. Tolédano, Phys. Rev. B **77**, 024109 (2008).
[77]P. B. Littlewood, J. Phys. C **13**, 4875 (1980).
[78]J. K. Burdett and T. J. McLarnan, J. Chem. Phys. **75**, 5764 (1981).
[79]J. K. Burdett, P. Haaland, and T. J. McLarnan, J. Chem. Phys. **75**, 5774 (1981).
[80]J. H. Bularzik, J. K. Burdett, and T. J. McLarnan, Inorg. Chem. **21**, 1434 (1982).
[81]T. A. Albright, J. K. Burdett, and M.-H. Whangbo, *Orbital Interactions in Chemistry* (Wiley, New York, 2011).
[82]X. N. Wu and F. Y. Wu, J. Phys. A **22**, L55 (1989).
[83]R. J. Baxter, *Exactly Solved Models in Statistical Mechanics* (Academic, New York, 1982).
[84]D. Vanderbilt and J. D. Joannopoulos, Phys. Rev. B **23**, 2596 (1981).
[85]Y. Shimoi and H. Fukutome, J. Phys. Soc. Jpn. **59**, 1264 (1990).
[86]A. V. Kolobov, P. Fons, A. I. Frenkel, A. L. Ankudinov, J. Tominaga, and T. Uruga, Nature Mater. **3**, 703 (2004).
[87]C. Steimer, V. Coulet, W. Welnic, H. Dieker, R. Detemple, C. Bichara, B. Beuneu, J. Gaspard, and M. Wuttig, Adv. Mater. **20**, 4535 (2008).
[88]J. K. Burdett and S. Lee, J. Am. Chem. Soc. **105**, 1079 (1983).
[89]J. B. Bersuker, *The Jahn-Teller Effect* (Cambridge University Press, Cambridge, England, 2006).
[90]E. Canadell and M.-H. Whangbo, Chem. Rev. **91**, 965 (1991).
[91]D. Seo and R. Hoffmann, J. Sol. State Chem. **147**, 26 (1999).
[92]M. J. Rice and E. J. Mele, Phys. Rev. Lett. **49**, 1455 (1982).
[93]P. Jóvári, I. Kaban, J. Steiner, B. Beuneu, A. Schöps, and M. A. Webb, Phys. Rev. B **77**, 035202 (2008).
[94]V. Lubchenko and P. G. Wolynes, J. Chem. Phys. **119**, 9088 (2003).
[95]D. Bevzenko and V. Lubchenko, J. Phys. Chem. B **113**, 16337 (2009).
[96]Y. Iwadate, T. Hattori, S. Nishiyama, K. Fukushima, Y. Mochizuki, M. Misawa, and T. Fukunaga, J. Phys. Chem. Solids **60**, 1447 (1999).
[97]*Semiconductors other than group IV elements and III-V compounds*, edited by O. Madelung (Springer-Verlag, Berlin, 1992).
[98]V. Lubchenko, Proc. Natl. Acad. Sci. U.S.A. **105**, 10635 (2008).
[99]R. A. Stern and G. F. Tuthill, Int. J. Mod. Phys. B **15**, 3331 (2001).
[100]P. Goldstein and A. Paton, Acta Cryst. B **30**, 915 (1974).
[101]NIST Scientific and Technical Databases, http://www.nist.gov/srd/index.htm.
[102]B. Cordero, V. Gomez, A. E. Platero-Prats, M. Reves, J. Echeverria, E. Cremades, F. Barragan, and S. Alvarez, Dalton Trans. **2008**, 2832 (2008).
[103]P. Pyykkö and M. Atsumi, Chem.- Eur. J. **15**, 186 (2009).
[104]Cambridge Crystallographic Data Centre, http://www.ccdc.cam.ac.uk/products/csd/radii/.
[105]M. Springborg and Y. Dong, Int. J. Quantum Chem. **109**, 837 (2009).
[106]P. Ghosh, J. Bhattacharjee, and U. V. Waghmare, J. Phys. Chem. C **112**, 983 (2008).
[107]J. J. P. Stewart, J. Mol. Model. **13**, 1173 (2007).
[108]M. J. S. Dewar and W. Thiel, J. Am. Chem. Soc. **99**, 4899 (1977).
[109]N. Bernstein, M. J. Mehl, and D. A. Papaconstantopoulos, Phys. Rev. B **66**, 075212 (2002).
[110]J. Moilanen, C. Ganesamoorthy, M. S. Balakrishna, and H. M. Tuononen, Inorg. Chem. **48**, 6740 (2009).
[111]M. H. Karimi-Jafari, M. Ashouria, and A. Yeganeh-Jabrib, Phys. Chem. Chem. Phys. **11**, 5561 (2009).
[112]I. N. Levine, *Quantum Chemistry*, 6th ed. (Prentice-Hall, Englewood Cliffs, NJ, 2009), p. 714.
[113]MOPAC2009 J. J. P. Stewart, Stewart Computational Chemistry, Colorado Springs, CO, USA, http://OpenMOPAC.net (2008).
[114]A. Bondi, J. Phys. Chem. **68**, 441 (1964).
[115]K. W. Klinkhammer and P. Pyykkö, Inorg. Chem. **34**, 4134 (1995).
[116]See supplementary material at http://dx.doi.org/10.1063/1.3511707 for an illustration of voids in crystalline As_2Se_3, image of Br crystal, and angular maps of the strength of the $pp\sigma$-interaction in selected substances.

Supplementary Material for Molecular basis of the glass transition in pnictide and chalcogenide semiconductor alloys. Part I: The mechanism of the $pp\sigma$-network formation.

by Andriy Zhugayevych and Vassiliy Lubchenko
Chemistry Department, University of Houston, TX 77204-5003
(Dated: June 3, 2010)

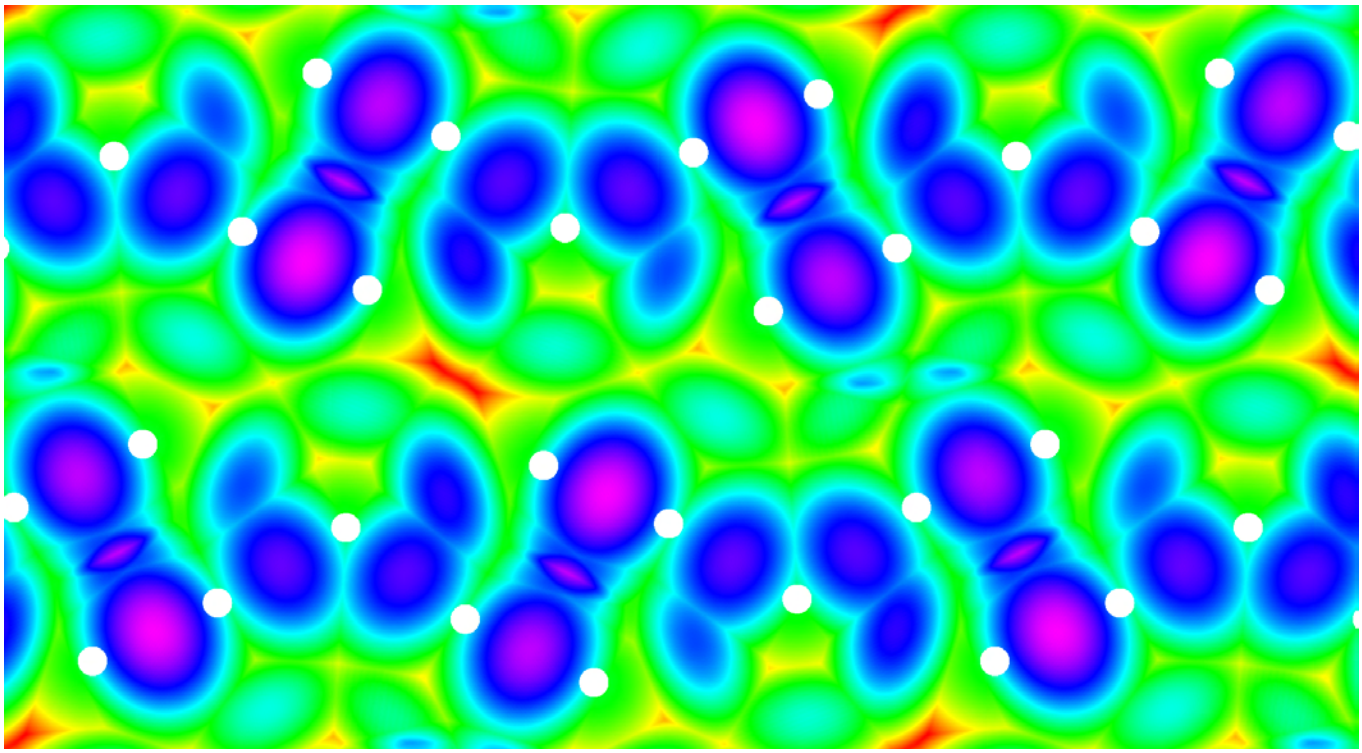

FIG. 1: Voids in As_2Se_3 crystal. The graph is generated as follows: First, we compute the distance $r_{\min}$ to the nearest atom in each point (ξ, η, ζ) in the lattice coordinates. (The lattice is monoclinic.) Call the resulting function $r_{\min}(\xi, \eta, \zeta)$. Next, we make a projection of this function onto the plane of Fig. 9 of the main text, which is perpendicular to the ζ axis, according to the following recipe. For each point (ξ, η), we vary ζ to find the largest value of $r_{\min}(\xi, \eta, \zeta)$, call it $r(\xi, \eta)$, and assign a color to the point (ξ, η) so that redder hues correspond to larger values of $r(\xi, \eta)$, more violet hues to smaller values of $r(\xi, \eta)$. The function $r(\xi, \eta)$ varies in the $[1.64, 2.52]$ Å range, while the sum of the covalent radii is 2.4 Å. As a result, intensely red regions mark voids in As_2Se_3 crystal. Atoms are marked by white balls. The largest void is distorted octahedral; it is centered at point $(1/2, 1/2, 1/2)$ with Se atoms as vertices.

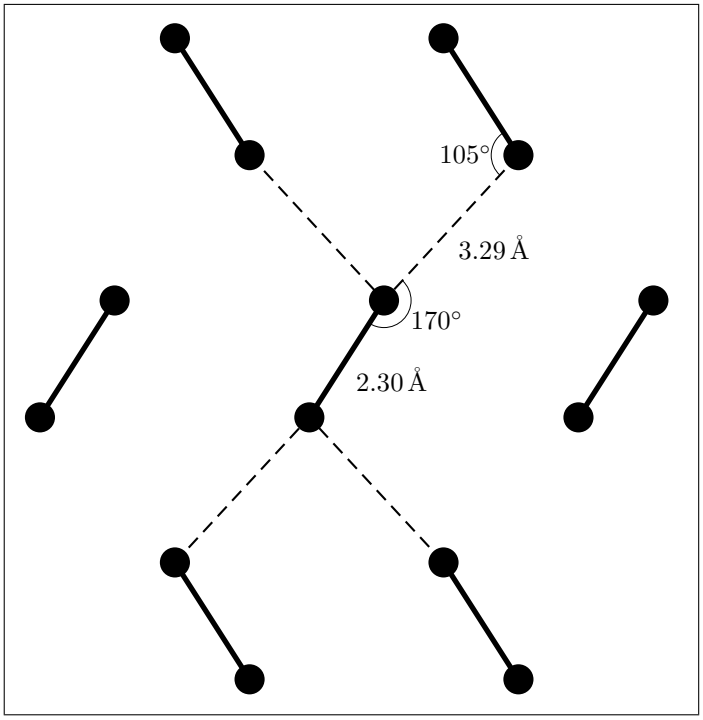

FIG. 2: Fragment of a slice of bromine crystal. Compare the bond angles with those in Fig. 3 of the main text.

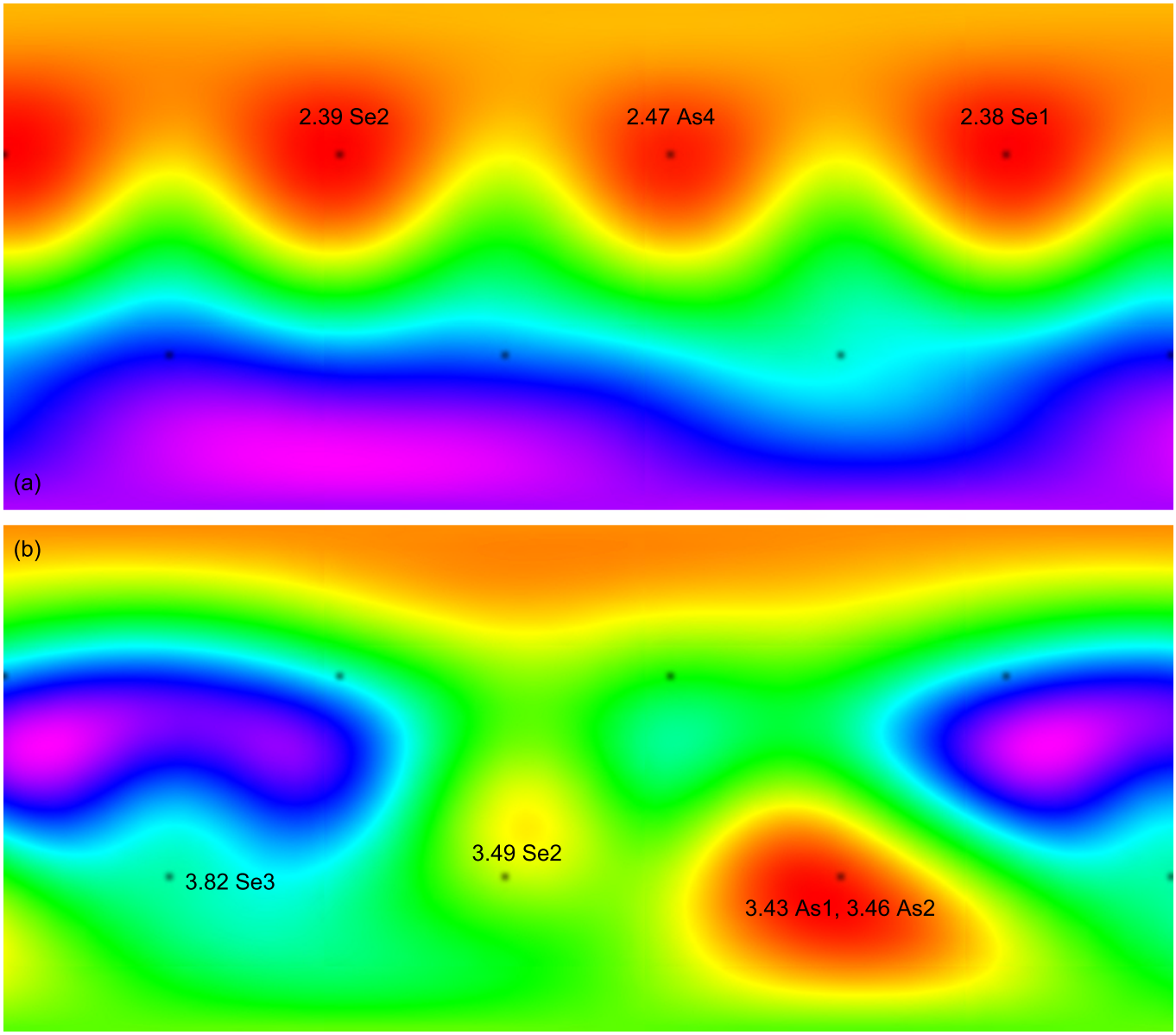

FIG. 3: Illustration of distorted octahedral coordination of the arsenic atom in the position As1 of As_4Se_4 crystal. Draw a sphere around the As1 atom at its covalent radius (1.2 Å). For each point, compute the logarithm of the sum of the radial parts of the p orbitals on the atoms within 4.5 Å. Assign a color to the value of this function so that redder hues correspond to larger values and more violet hues to smaller values. The resulting map is Merkator-projected on a rectangular area, where the top edge corresponds to the north pole. The resulting map is shown in panel (a). In perfect octahedral coordination, red areas would be centered at the black dots. (The line connecting the poles coincides with a C_3 axis of the octahedron.) In panel (b), the nearest neighbors are excluded, to specifically highlight back-bonding. The pertinent neighbors are indicated, together with their distance to the As1 atom, in Angstroms.

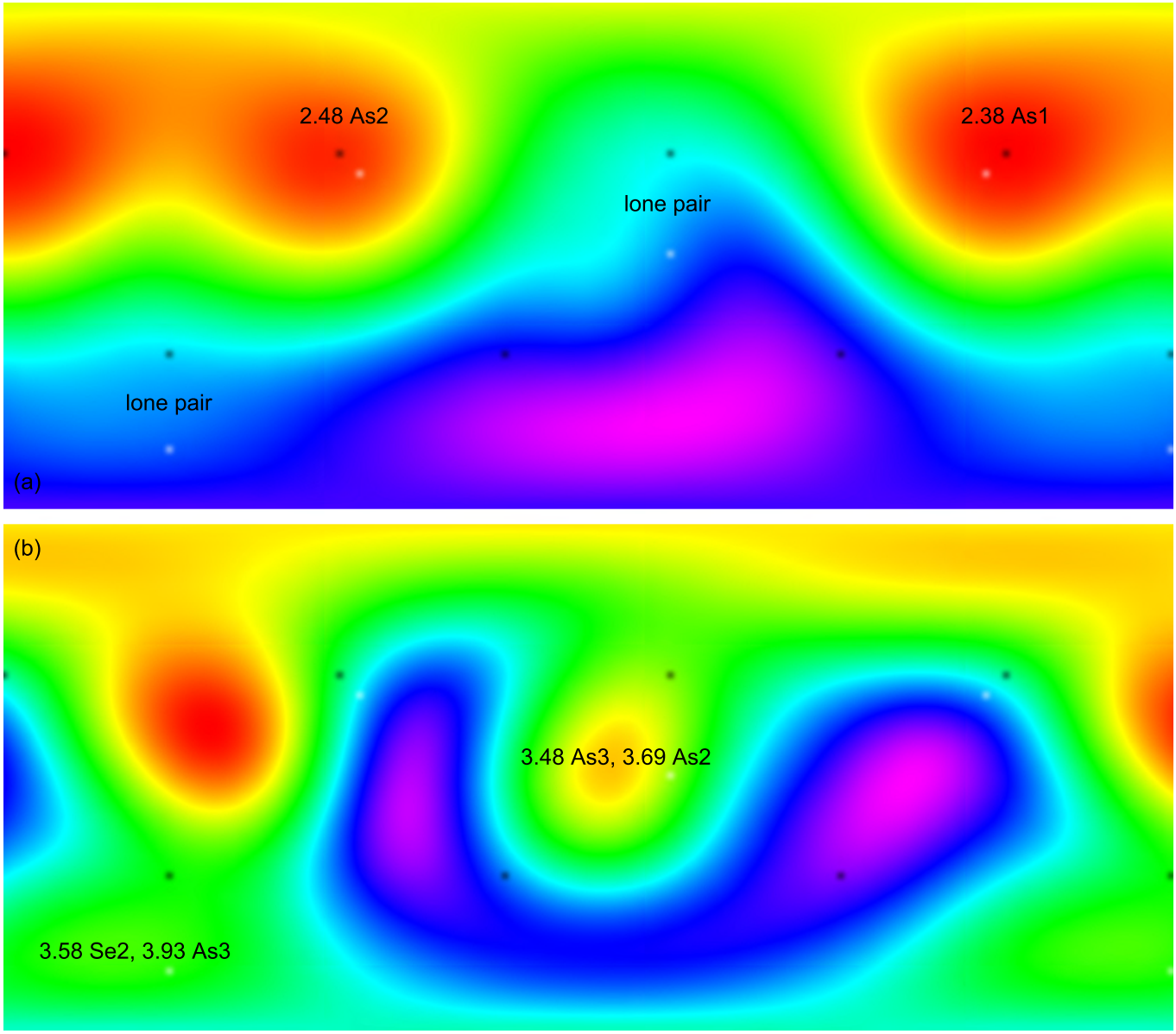

FIG. 4: Distorted tetrahedral coordination of the selenium atom in the position Se1 of As_4Se_4 crystal. See Fig. 3 for explanation. Black and white dots indicate octahedral and tetrahedral coordination respectively.

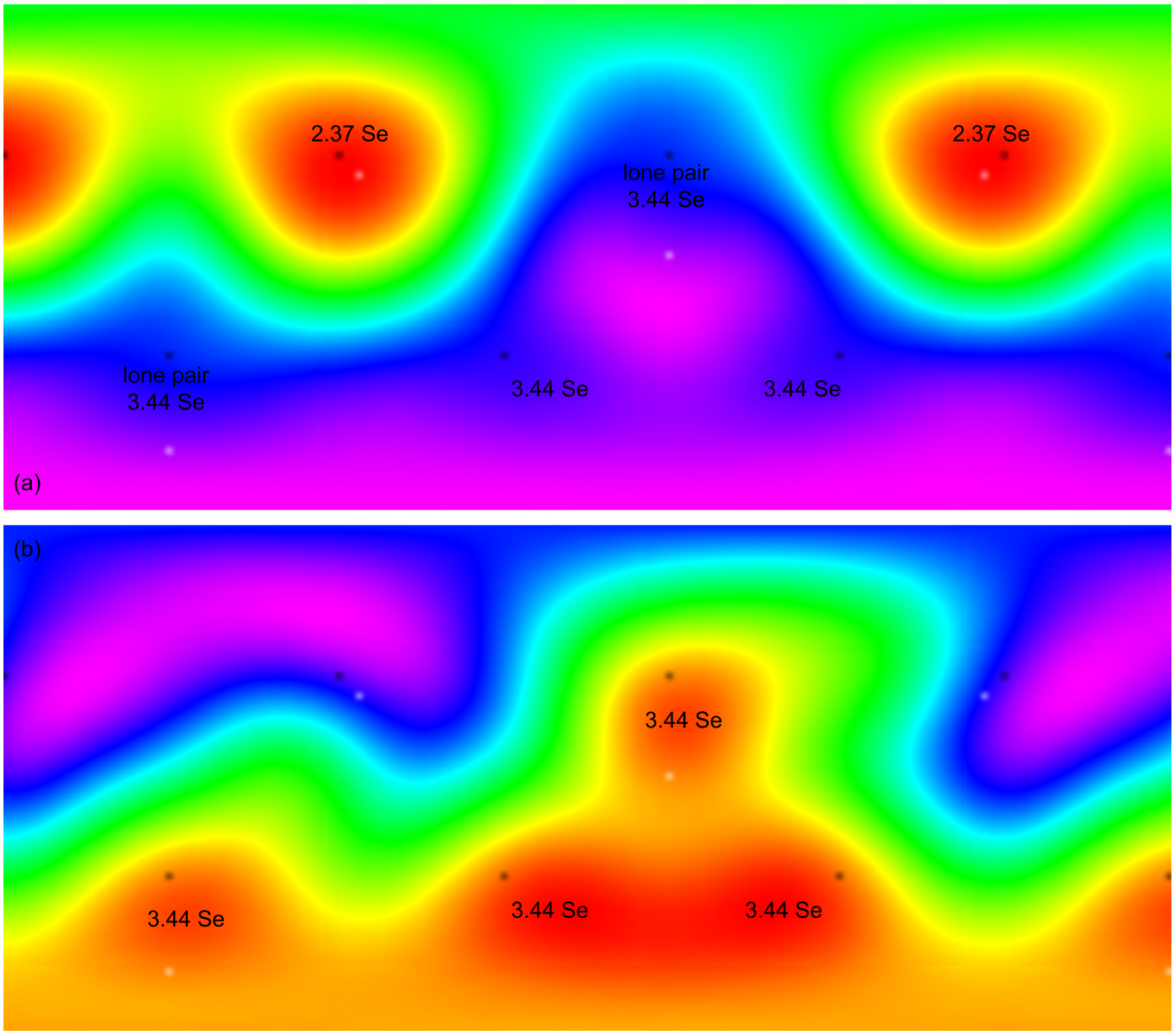

FIG. 5: Distorted octahedral coordination of the atoms in trigonal-Se crystal. See Figs. 3 and 4 for explanation.